Electronic Supplementary Material (ESI) for Catalysis Science & Technology.

Supporting Information

Single-Step Benzene Hydroxylation by Cobalt(II) Catalysts via Co(III)-Hydroperoxo Intermediate

Karunanithi Anandababu,[a] Sethuraman Muthuramalingam,[a] Marappan Velusamy,[b] and Ramasamy Mayilmurugan*[a]

[a]Bioinorganic Chemistry Laboratory/ Physical Chemistry, School of Chemistry, Madurai Kamaraj University, Madurai 625 021, Tamil Nadu, India.
E-mail: mayilmurugan.chem@mkuniversity.org

[b]Department of Chemistry, North Eastern Hill University, Shillong-793022, India.

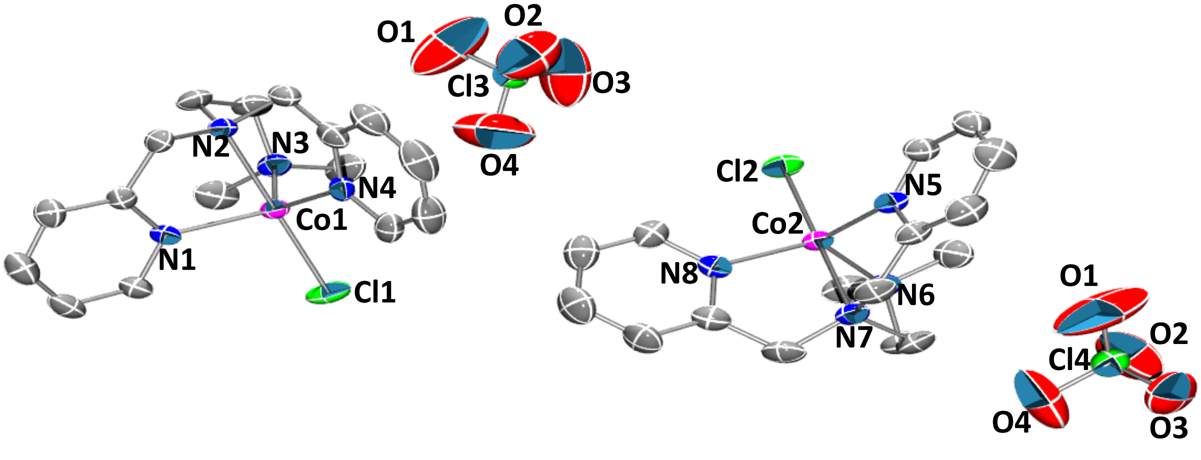

Figure S1. ORTEP view of Complex **1** with one counter ion (ClO_4^-) out of the coordination sphere.

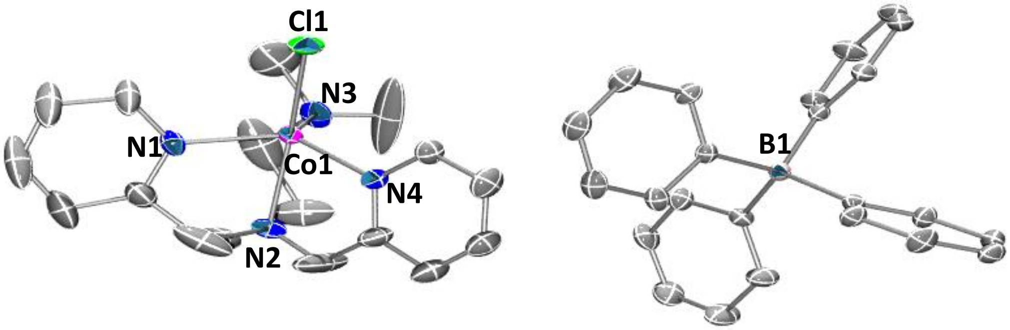

Figure S2. ORTEP view of Complex **2** with one counter ion (BPh_4^-) out of the coordination sphere.

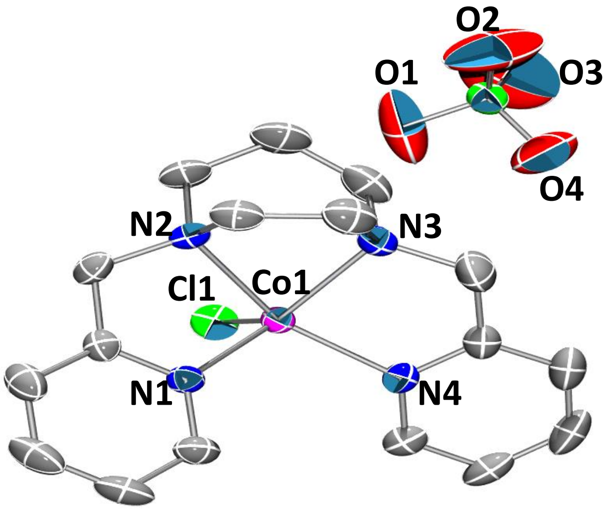

Figure S3. ORTEP view of Complex **4** with one counter ion (ClO_4^-) out of the coordination sphere.

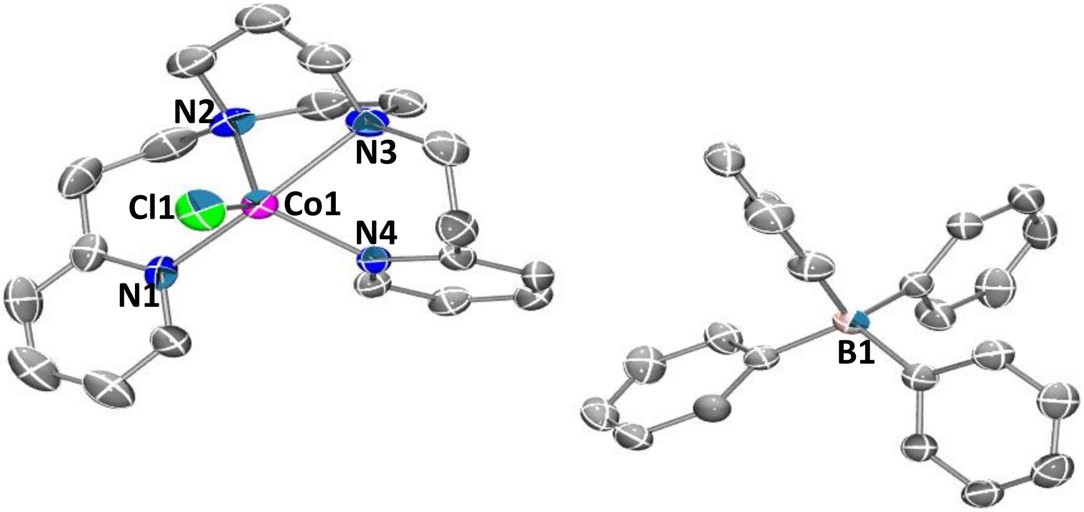

Figure S4. ORTEP view of Complex **5** with one counter ion (ClO_4^-) out of the coordination sphere

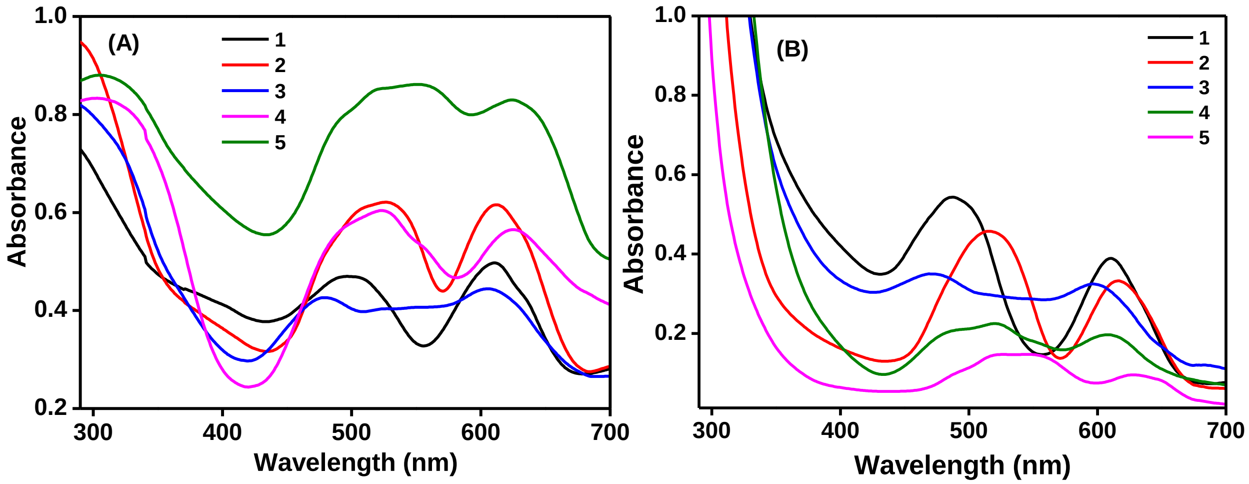

Figure S5. Electronic spectra of complexes **1** – **5** in solid state (A). Electronic spectra of complexes **1** – **5** (5×10^{-3} M) in acetonitrile at 25 °C (B).

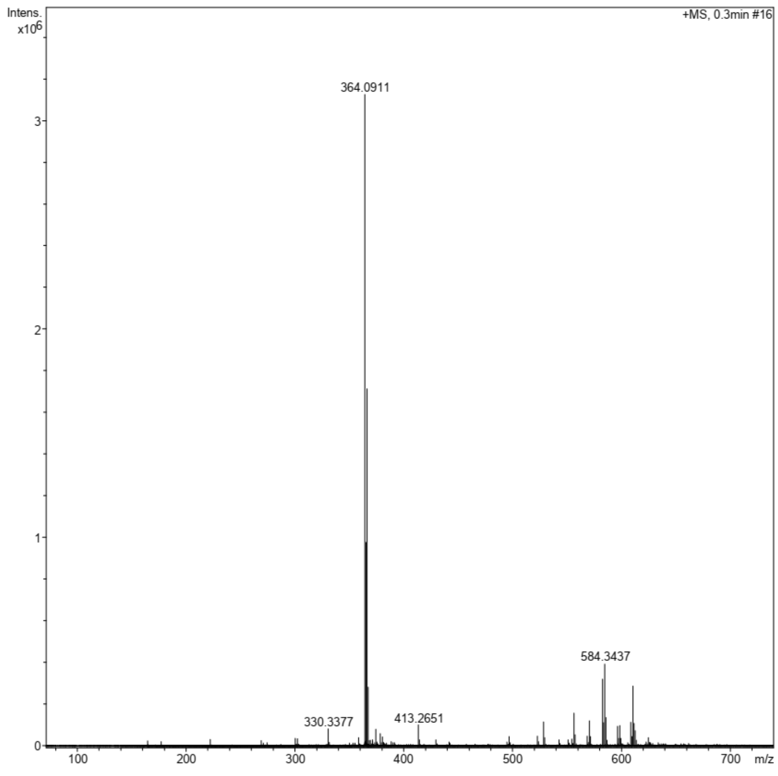

Figure S6. HR-ESI mass spectrum of complex **1** in Acetonitrile.

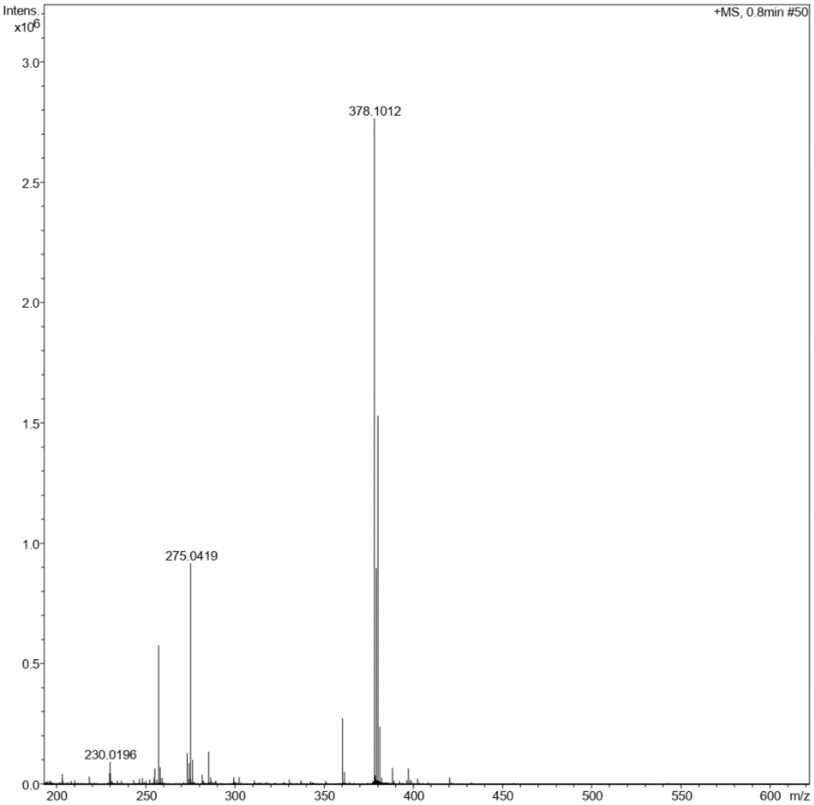

Figure S7. HR-ESI mass spectrum of complex **2** in Acetonitrile.

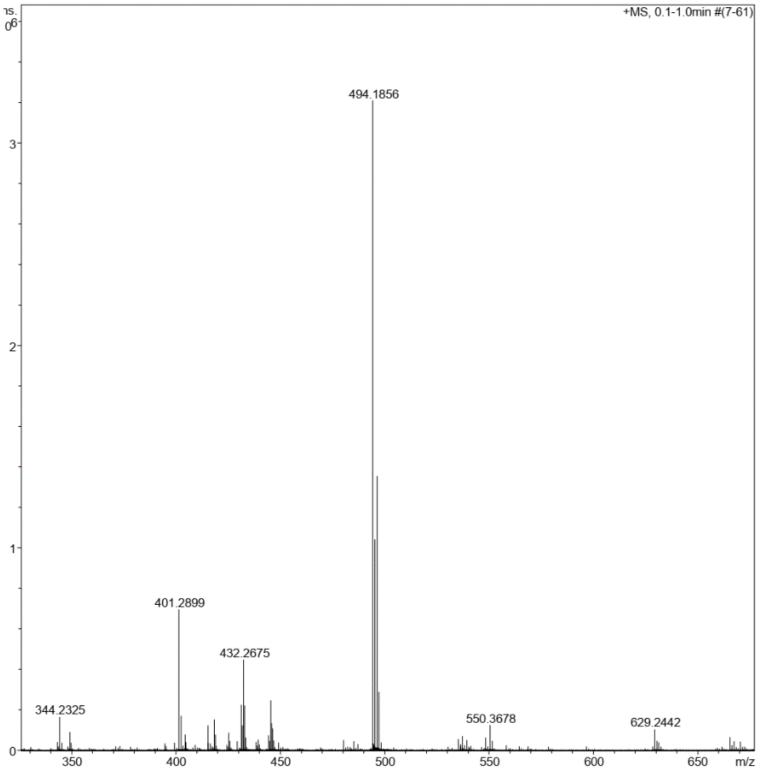

Figure S8. HR-ESI mass spectrum of complex **3** in Acetonitrile.

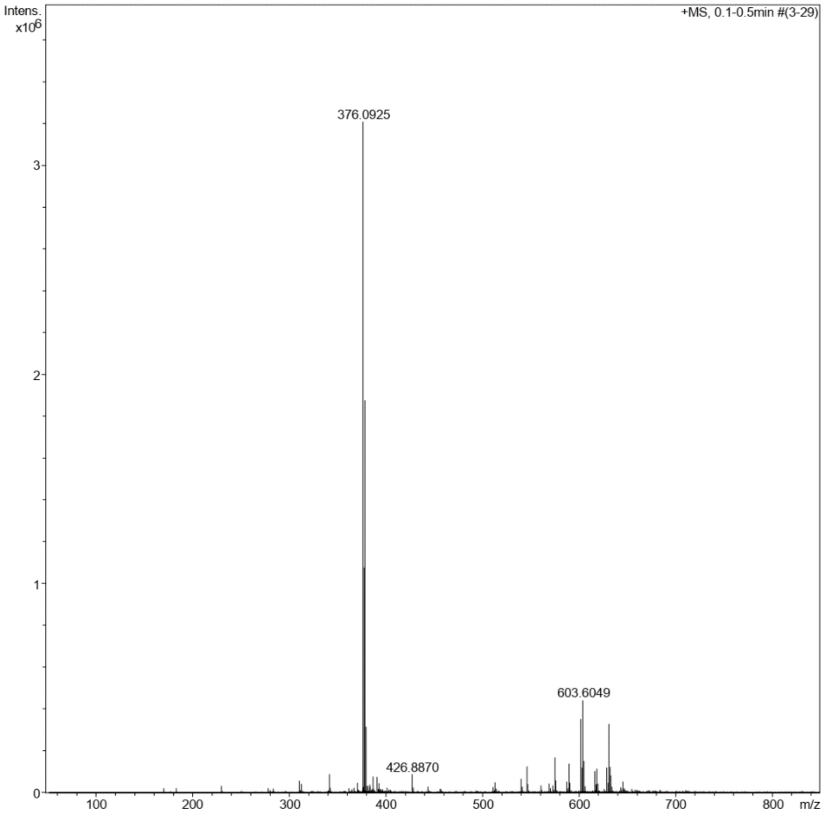

Figure S9. HR-ESI mass spectrum of complex **4** in Acetonitrile.

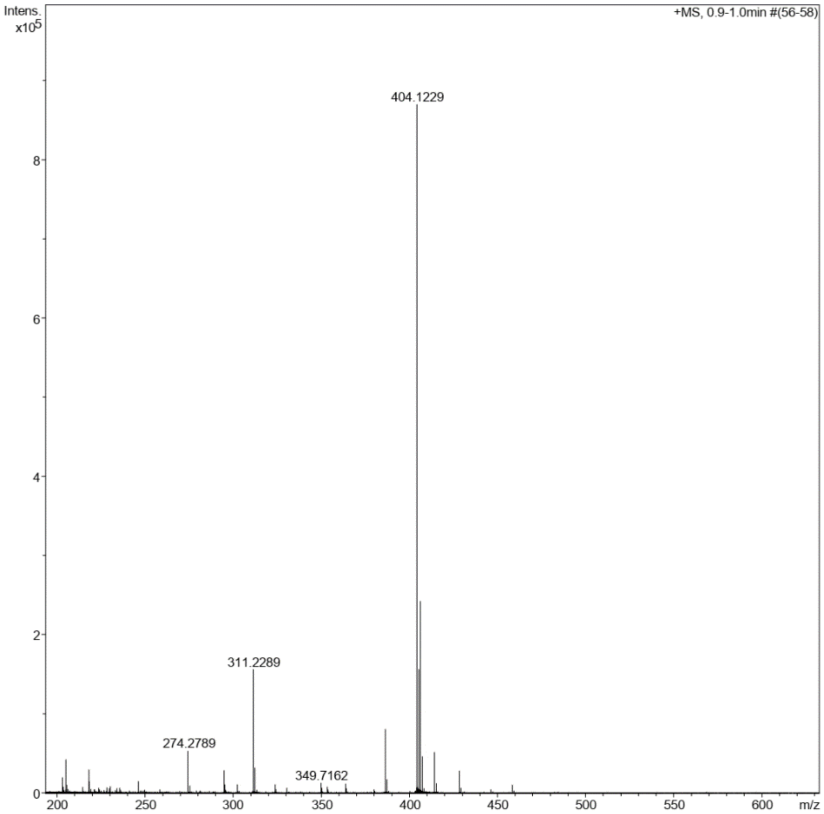

Figure S10. HR-ESI mass spectrum of complex **5** in Acetonitrile.

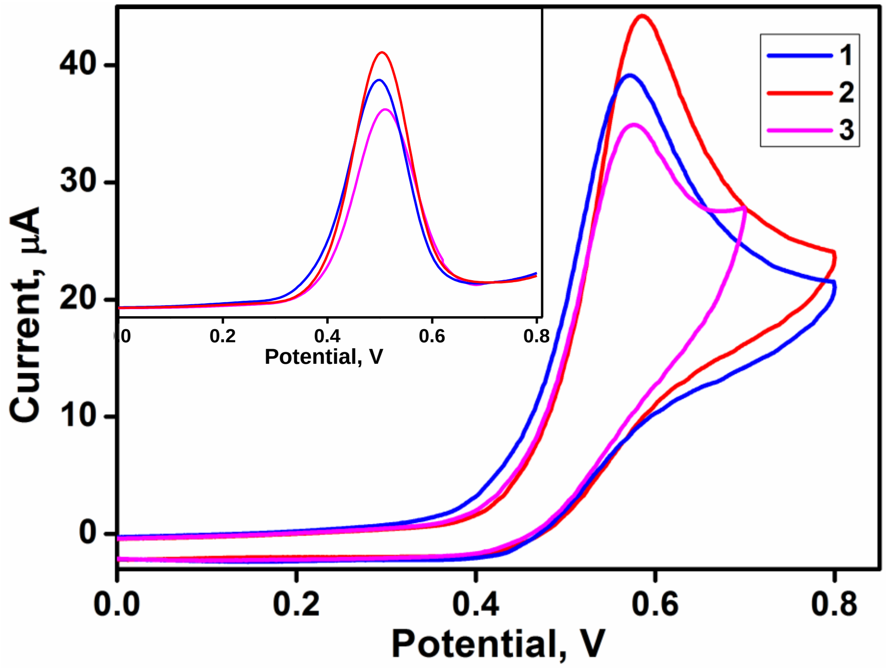

Figure S11. Cyclic Voltammograms and DPV (Insert) of **1 - 3** (1 ×10^{-3} M) at 25 ˚C in acetonitrile. Supporting electrolyte: NBu_4PF_6 (0.1 M). Reference: Ag/Ag^+; working electrode: Pt-sphere; Counter electrode: Pt wire; scan rate = 100 mV s^{-1}. Insert: DPV for **1- 3**

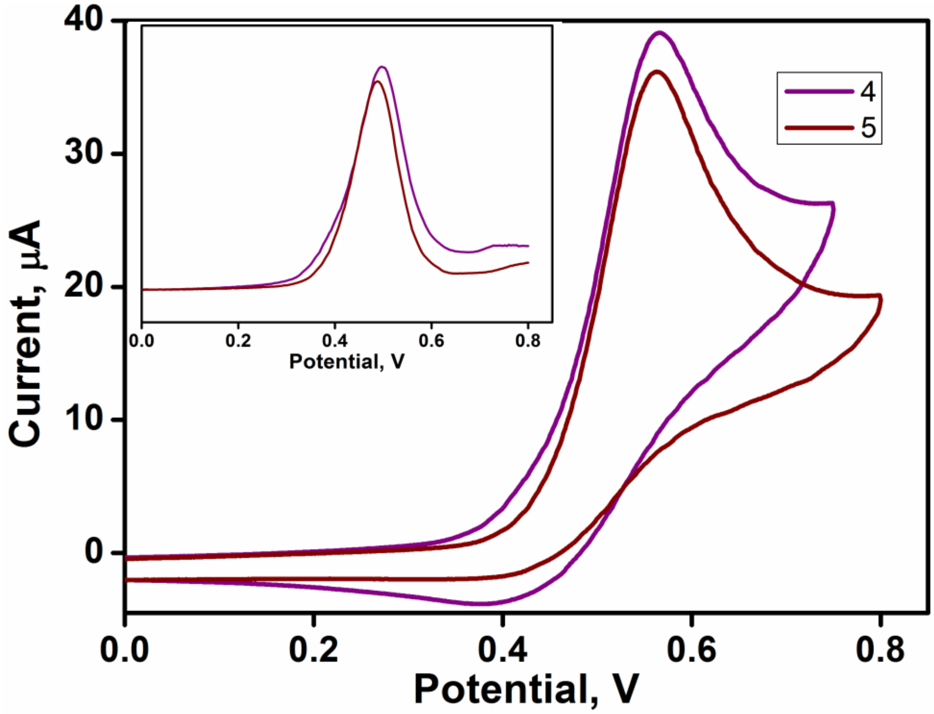

Figure S12. Cyclic Voltammograms of **4** and **5 (**2 ×10^{-3} M) at 25 ˚C in acetonitrile. Supporting electrolyte: NBu_4PF_6 (0.2 M). Reference: Ag/Ag^+; working electrode: Pt-sphere; Counter electrode: Pt wire; scan rate = 100 mV s^{-1}. Insert: DPV for **4** and **5**.

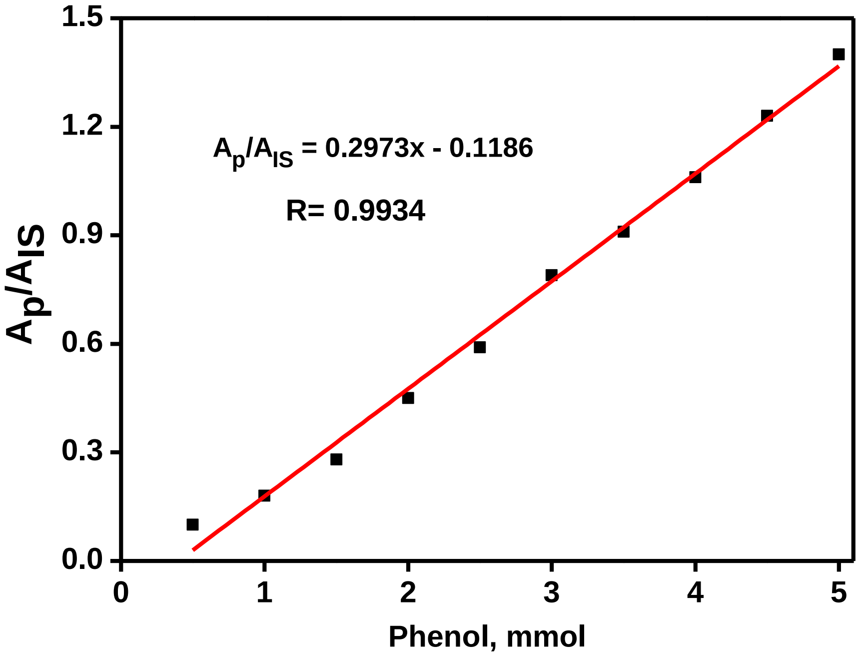

Figure S13. The standard calibration curve using GC, area ratio of phenol to the internal standard (nitrobenzene) (A_P/A_{IS})[a]. [a]A is designated as the chromatographic peak area; p stands for phenol and IS stands for internal standard (nitrobenzene).

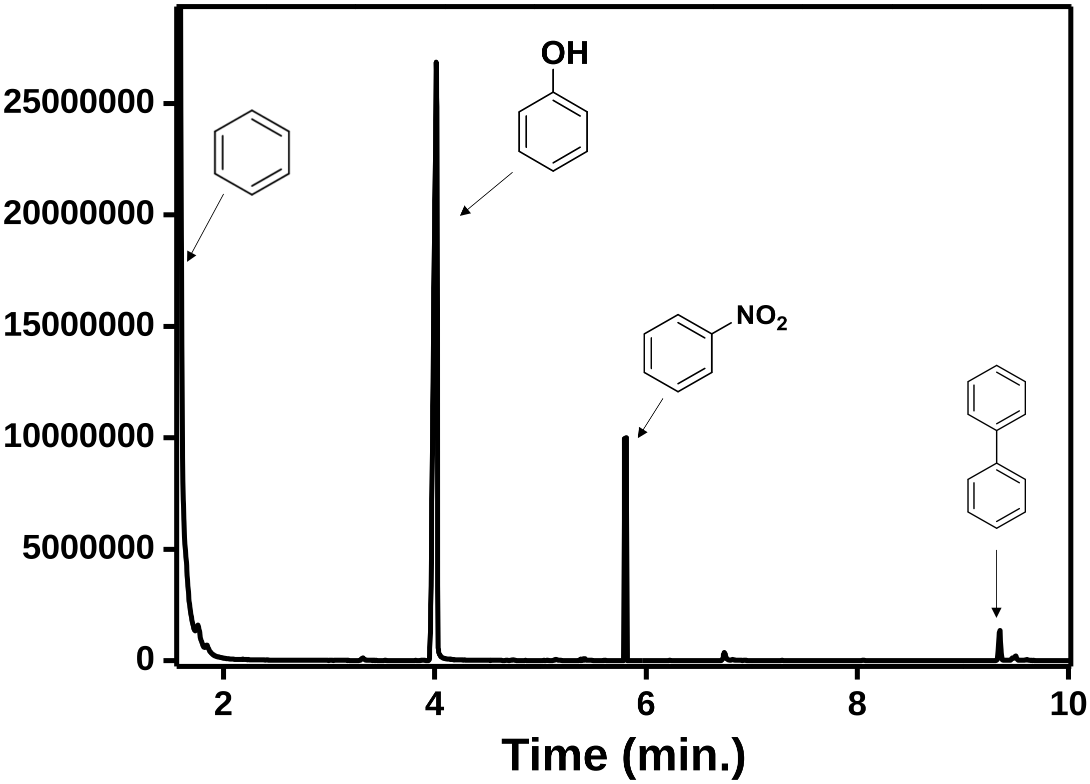

Figure S14. GC-MS of benzene to phenol conversion by **3** as catalyst (5 μM), C_6H_6 (5 mmol), H_2O_2 (25 mmol) at 60 °C.

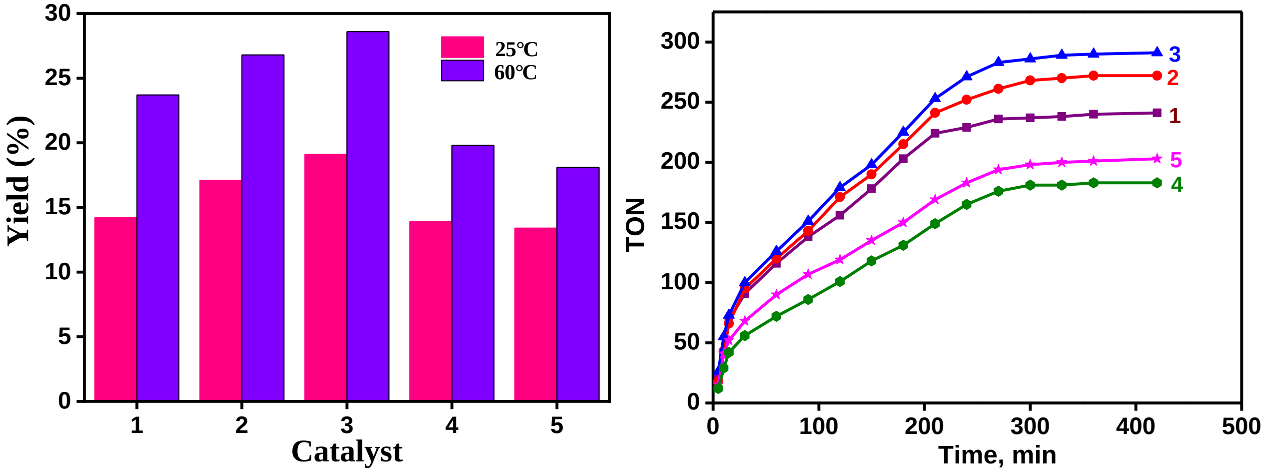

Figure S15. Bar diagram for the phenol formation catalyzed by **1 – 5** (5 μmol) using H_2O_2 (25 mmol) in acetonitrile at 25 °C /60 °C (A). The plot of time vs TON for the catalytic oxidation of benzene (5 mmol) with H_2O_2 (25 mmol) by **1 – 5** at 60 °C (B).

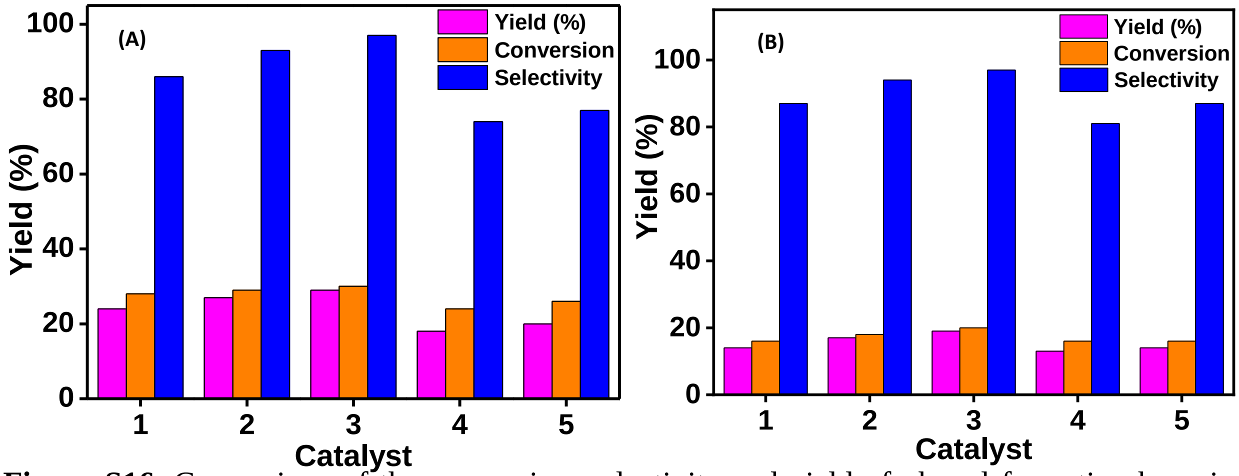

Figure S16. Comparison of the conversion, selectivity and yield of phenol formation by using catalyst **1 – 5** at 60 °C (**A)** and 25 °C **(B)** in the presence of aqueous H_2O_2 (25 mmol).

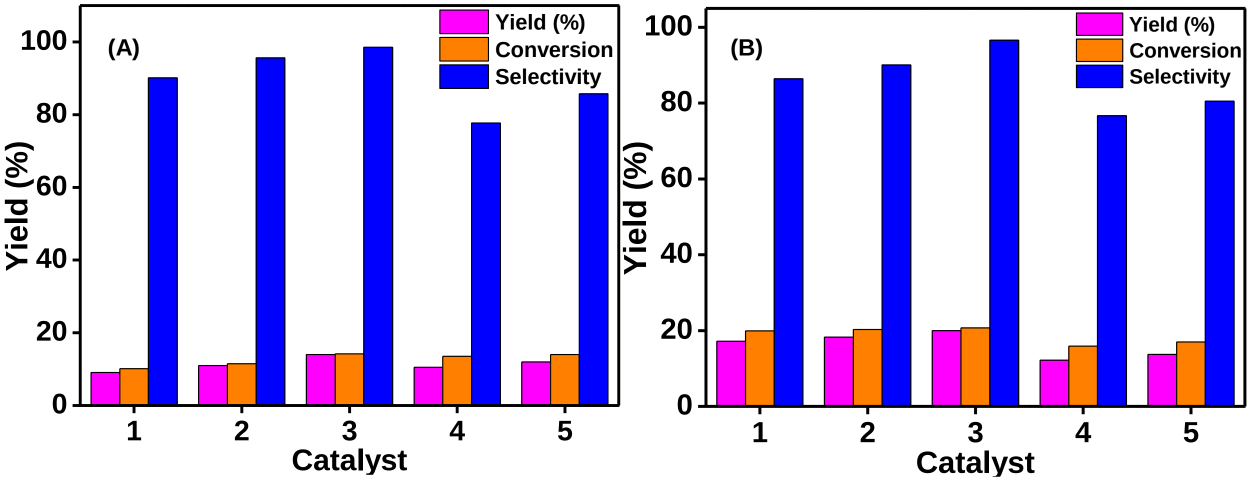

Figure S17. Variation of the conversion, selectivity and yield of phenol formation by **1 - 5** at 25 °C (**A)** and 60 °C **(B)** in the presence of aqueous H_2O_2 (5 mmol).

Calculation of Steric Maps

To build the steric map, the overall complex was oriented in a Cartesian frame with a selected point at the origin, a second point along the z-axis, and a third point in the xz plane. These three points are understood as corresponding to an atom or to the midpoint of a chosen subset of atoms. After alignment of the complex, atoms that must be excluded from the steric map calculations were removed, and the first coordination sphere around the metal was analyzed. After the complex was oriented and the selected atoms were removed, a sphere of radius R, centered at the origin, is sectioned by a regular three-dimensional cubic mesh of spacing s, which defines cubic voxels v. The distance between the center of each voxel with all the atoms in the ligand was tested to check if any of the atoms were within the van der Waals distance from the center of the examined voxel. If no atom was within the van der Waals distance, the examined voxel was marked as a free voxel, and otherwise the examined voxel was marked as buried. After all the voxels in the sphere are marked as free or buried for each (x,y) point within the first coordination sphere, the program scans the sphere from the top (i.e., from positive z-values) to determine the z-value of the first buried voxel. This procedure results in a surface defined as $S(x,y) = z_B$, which represents the surface of the ligand that is exposed toward the incoming reactants. In other words, this $S(x,y) = z_B$ surface defines the shape of the reactive pocket. Positive values of z_B indicate that the ligands protrude in the $z > 0$ half sphere, which is the half-sphere where the reacting groups are placed.

Steric maps were obtained using the SambVca 2.1A web application, which can be found at https://www.molnac.unisa.it/OMtools/sambvca2.1/ index.html.

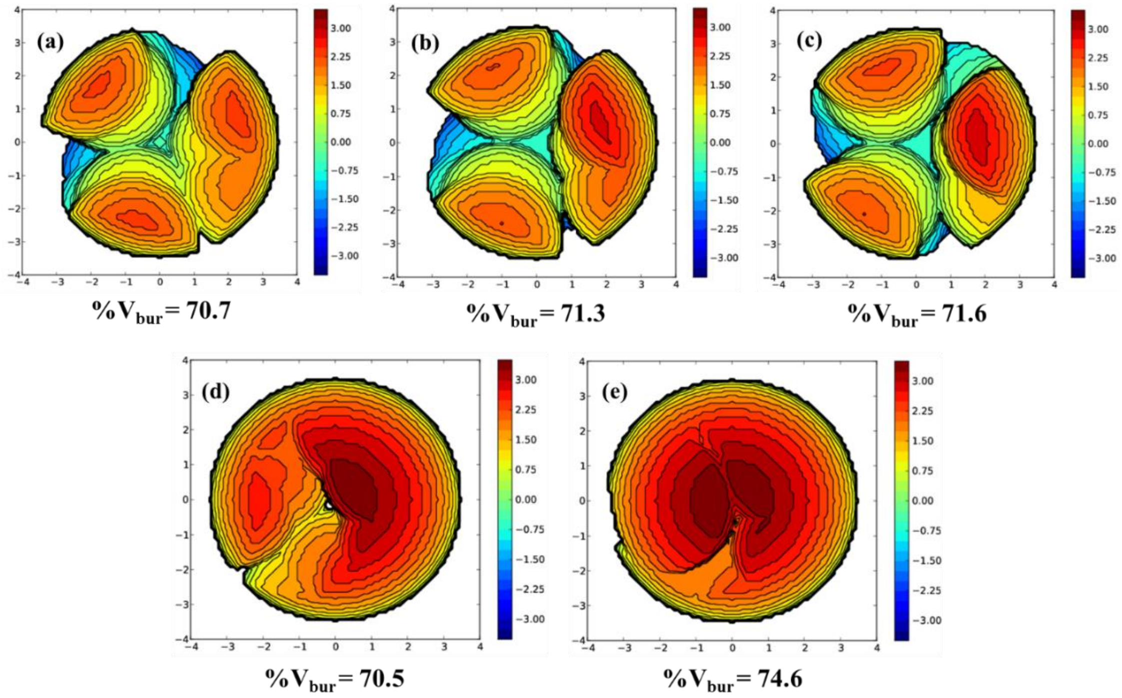

Figure S18. Steric maps of **1**(a), **2**(b), **3**(c), **4**(d), **5**(e) with %V$_{bur}$ calculated by SambVac 2.1A Web Application.

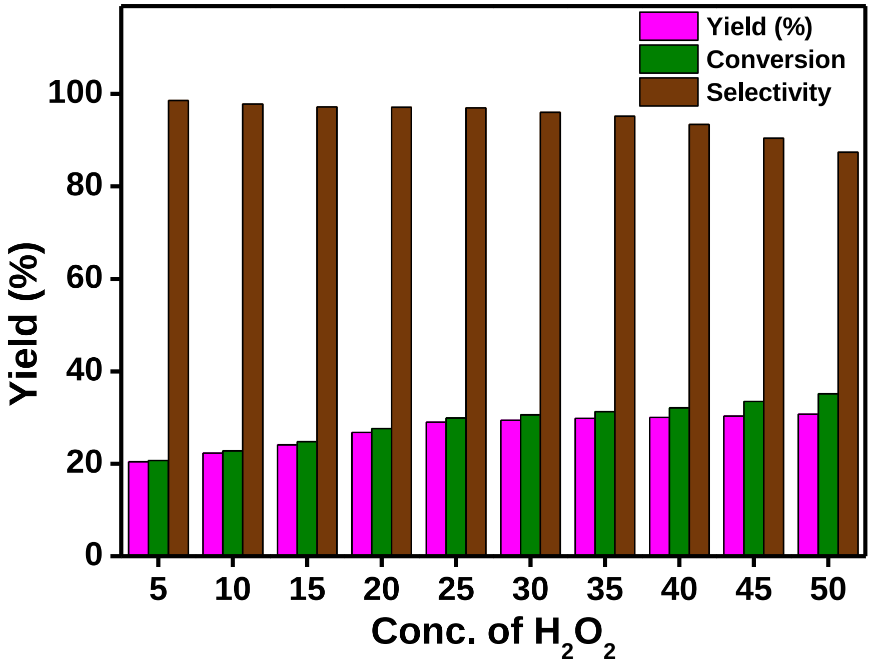

Figure S19. Phenol production vs. concentration of [H_2O_2] (5 – 50 mmol).

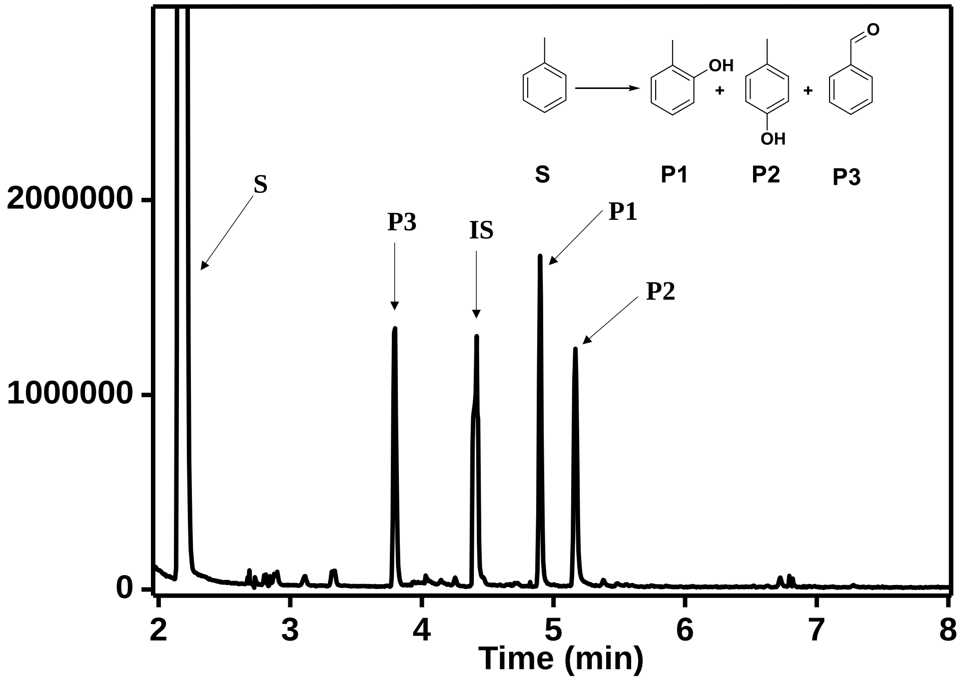

Figure S20. GC trace of the final reaction mixture of toluene oxidation.

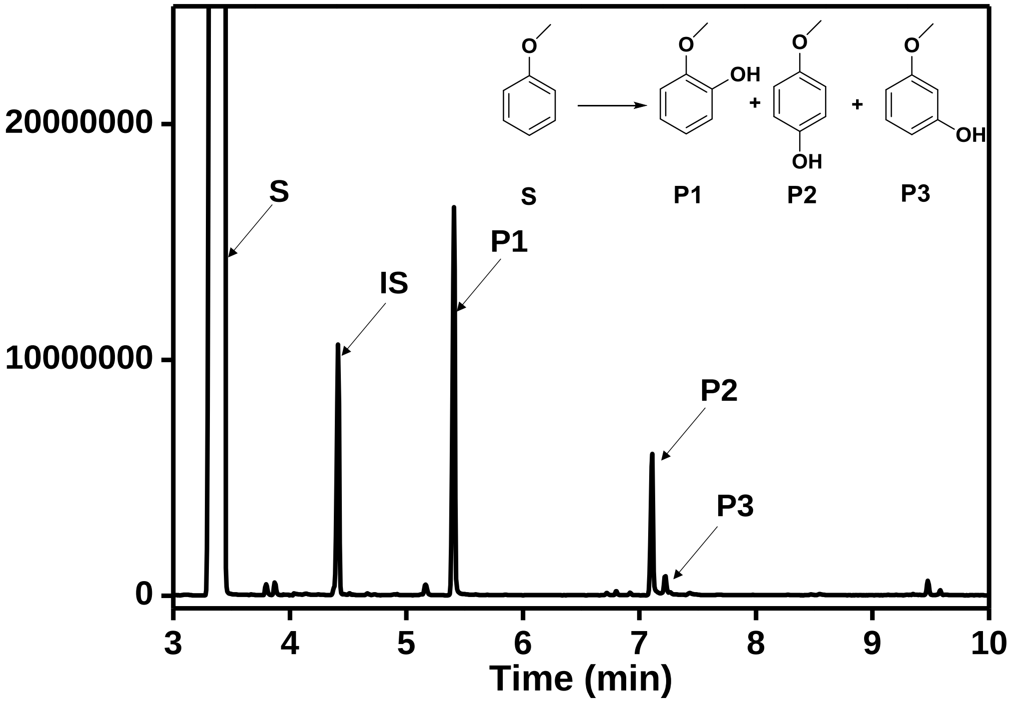

Figure S21. GC trace of the final reaction mixture of anisole oxidation.

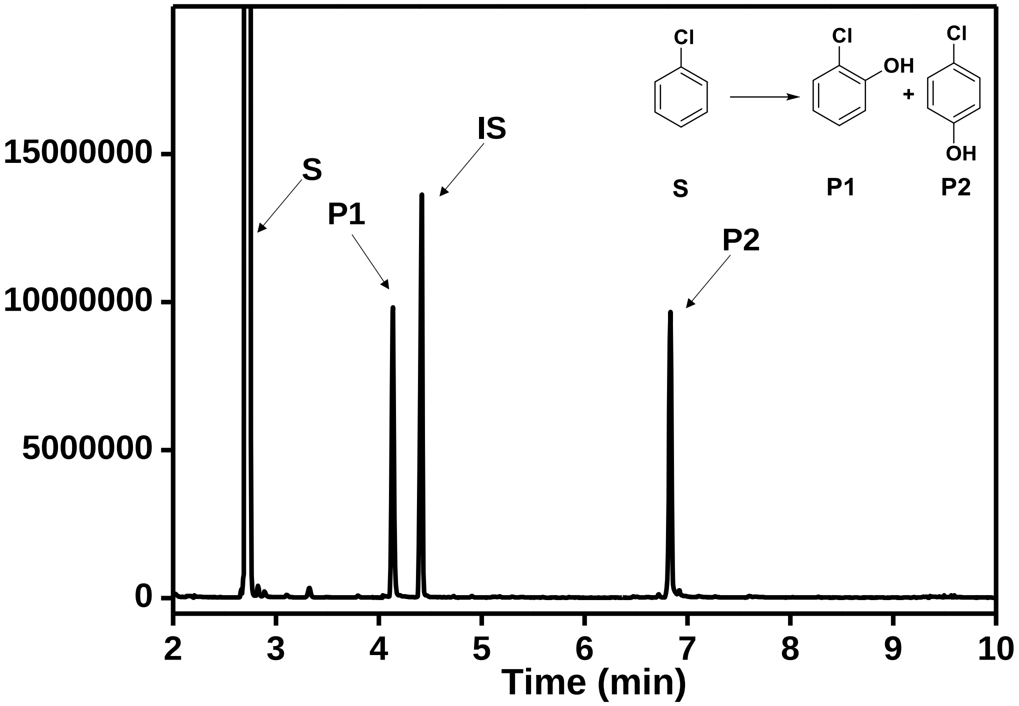

Figure S22. GC trace of the final reaction mixture of chlorobenzene oxidation.

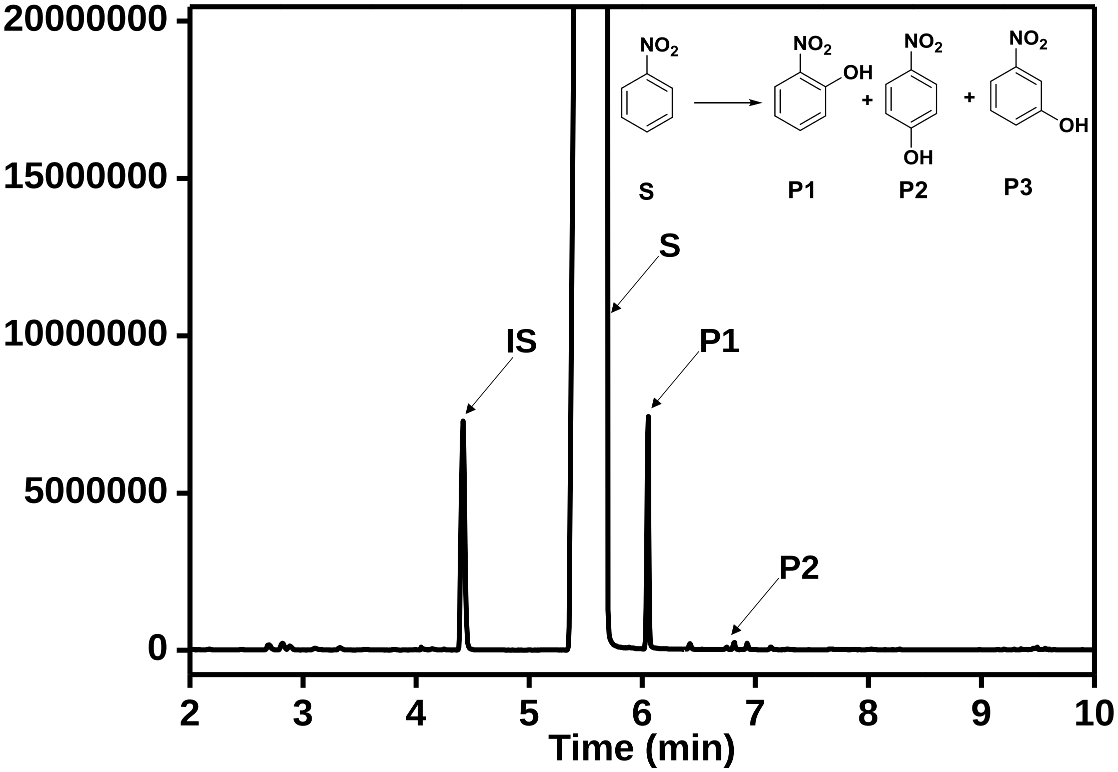

Figure S23. GC trace of the final reaction mixture of nitrobenzene oxidation.

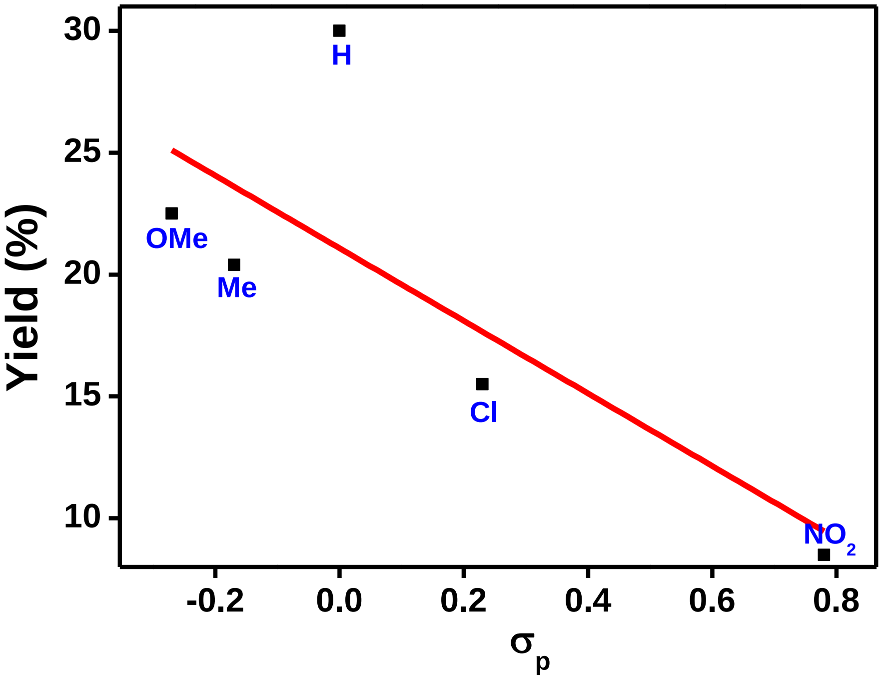

Figure S24. Hammett correlations of mono-substituted benzene hydroxylation using complex **3.**

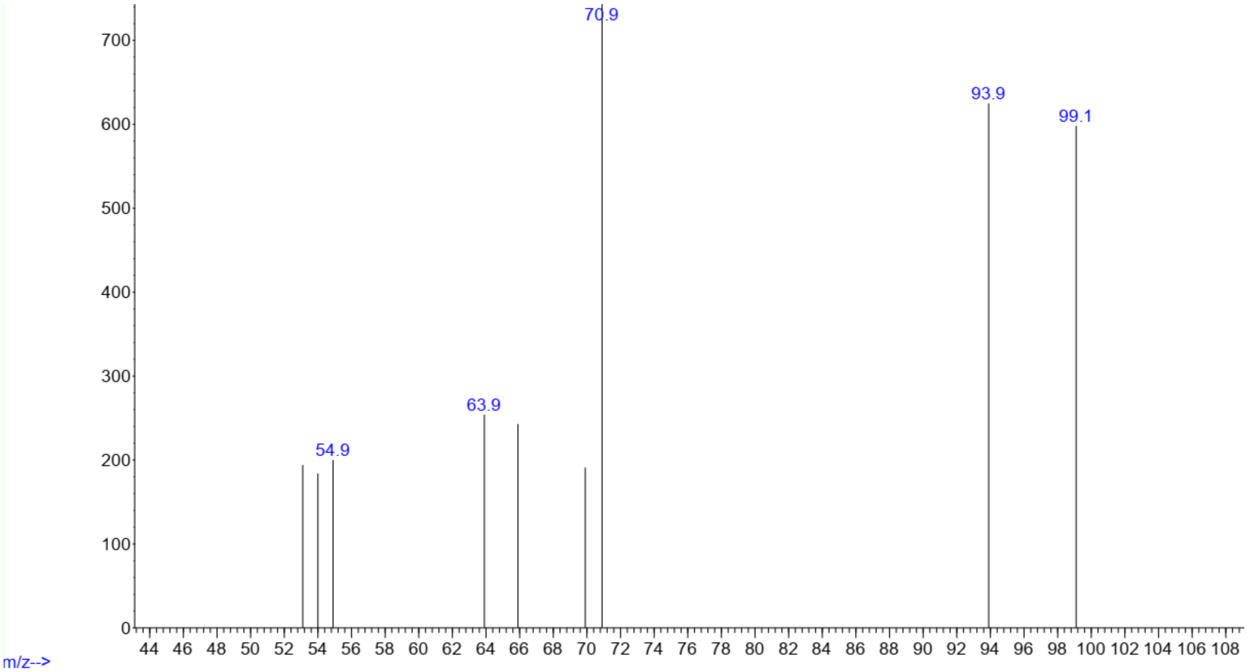

Figure S25. GC-MS profile for the measurement of KIE using C_6H_6 (2.5 mmol) and C_6D_6 (2.5 mmol) and **3** is employed as catalyst 25 mmol of H_2O_2 at 60 °C in 30 minutes.

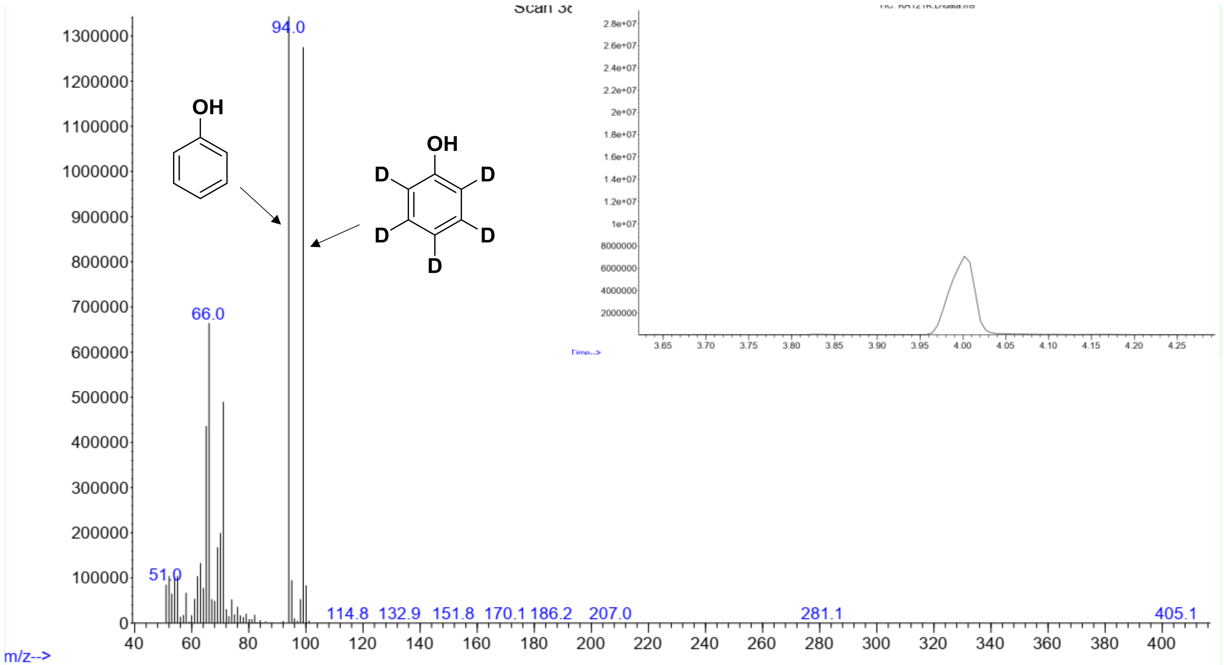

Figure S26. GC-MS profile for the measurement of KIE using C_6H_6 (2.5 mmol) and C_6D_6 (2.5 mmol) and **3** is employed as catalyst 25 mmol of H_2O_2 at 60 °C in 24 hours.

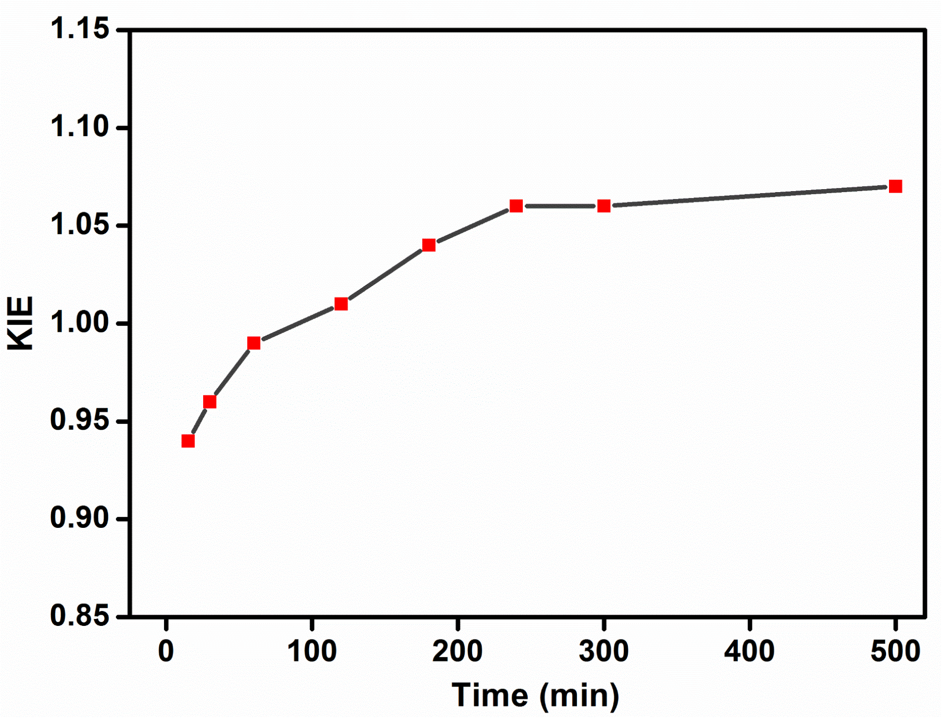

Figure S27. Plot of Time vs KIE using C_6H_6 (2.5 mmol) and C_6D_6 (2.5 mmol) and **3** is employed as catalyst 25 mmol of H_2O_2 at 60 °C in different time interval.

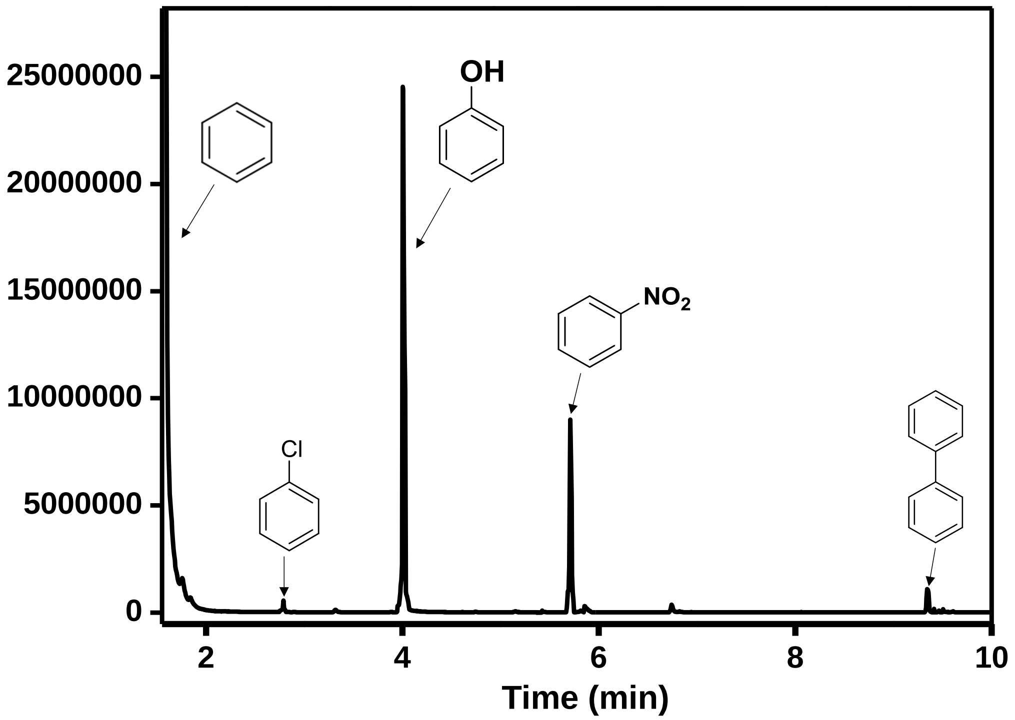

Figure S28. GC trace of the benzene hydroxylation reaction in the presence of CCl_4 as additive using catalyst **3**.

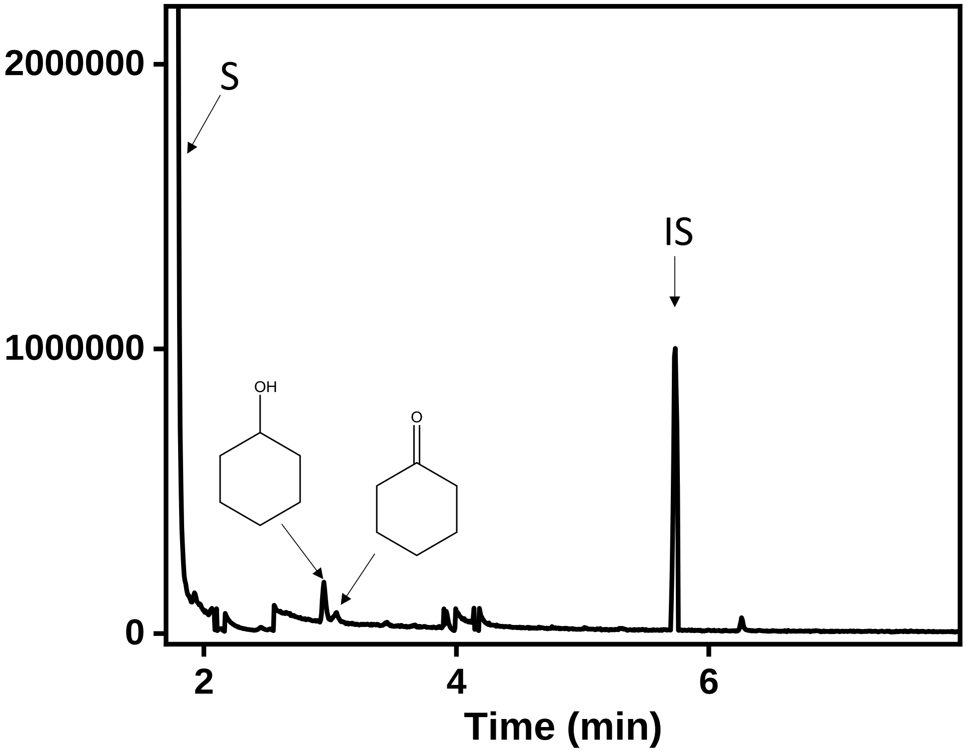

Figure S29. GC trace of the cyclohexane hydroxylation reaction in the presence of CCl_4 as additive using catalyst **3**.

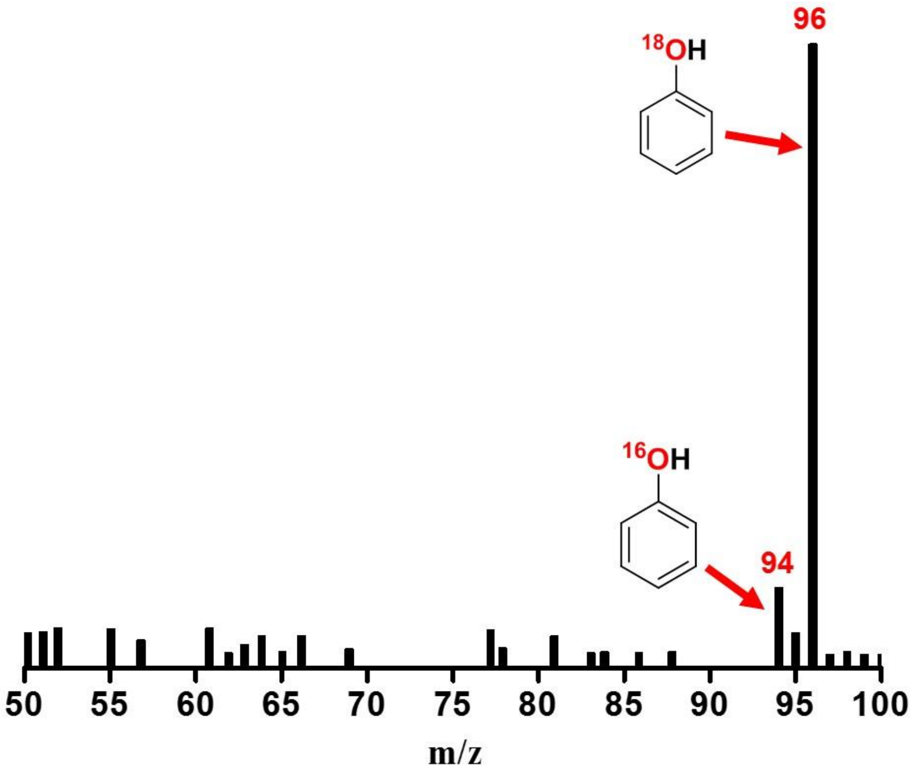

Figure S30. Isotopic studies for the reaction of **3** with using $H_2{}^{18}O_2$.

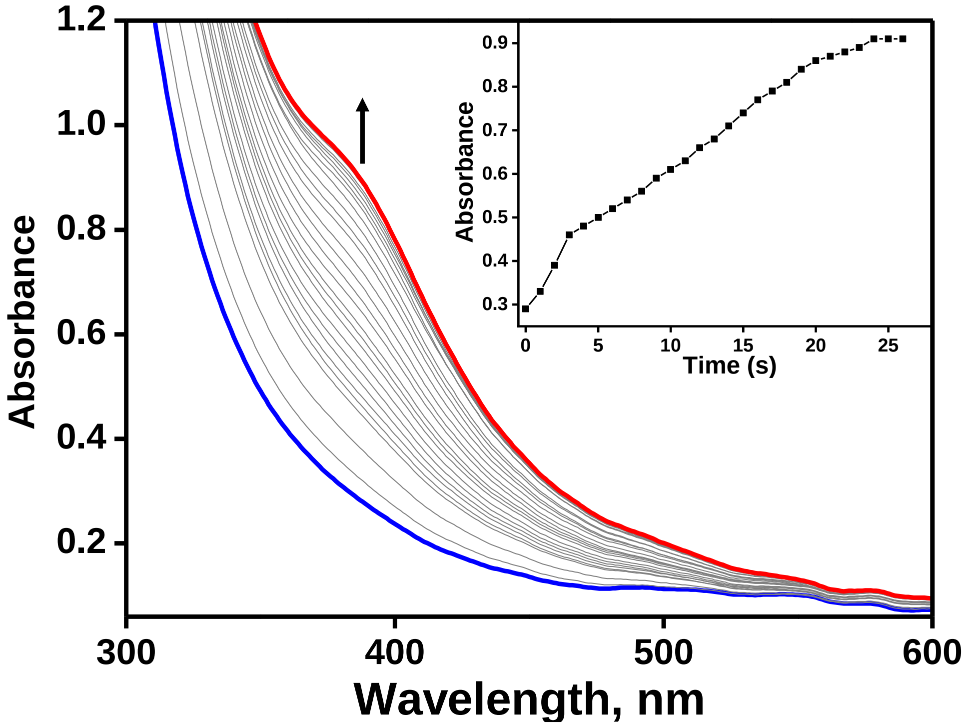

Figure S31. Electronic spectral changes for the reaction of **3** (4×10^{-4} M) with 2 equivalents of Et_3N and 10 equivalents of H_2O_2 at -40 °C in acetonitrile solution. Insert: plot of absorbance at 385 nm vs. time.

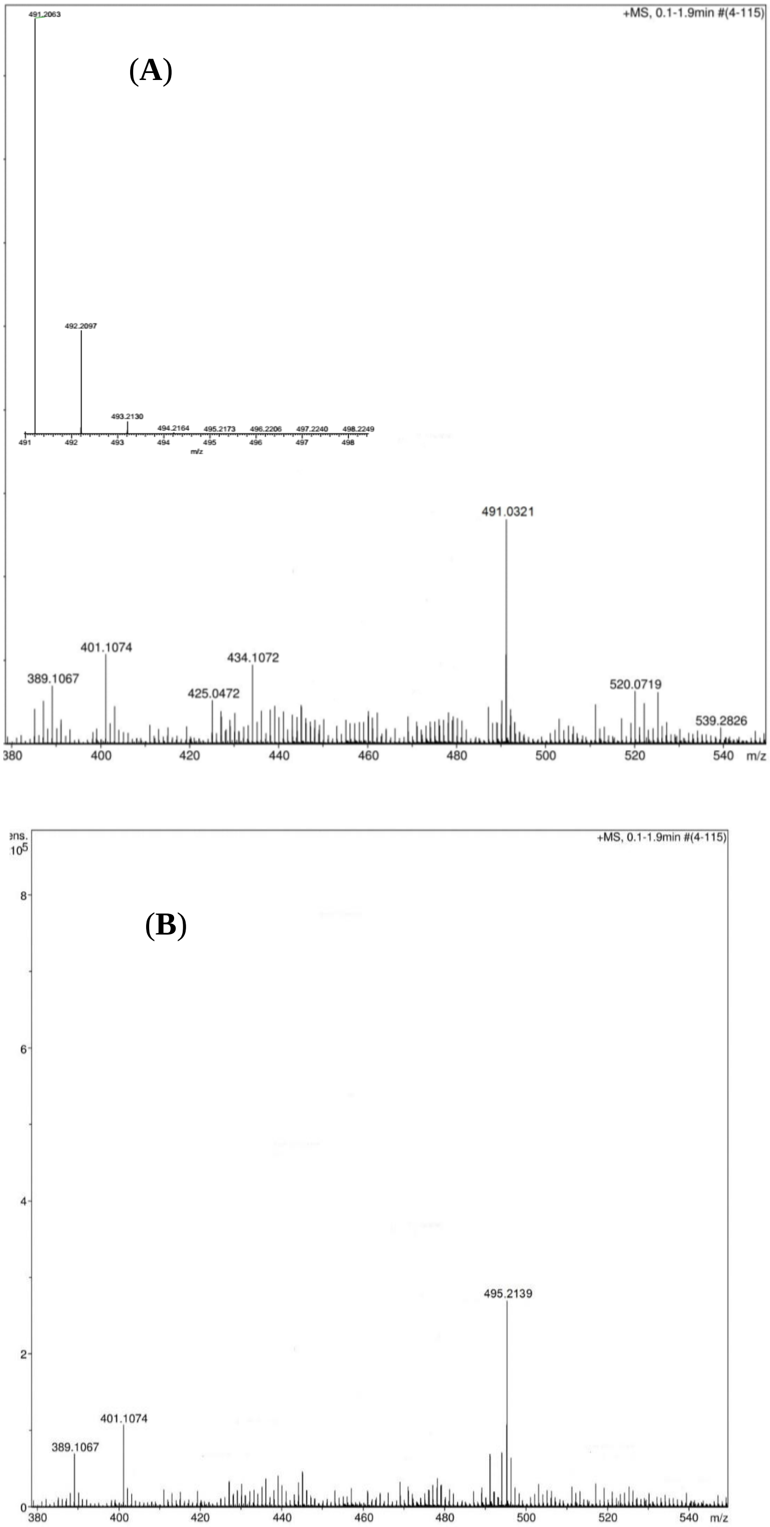

Figure S32. HR-ESI spectra of $[(L3Co^{III}\ (^{16}O_2)]^+$ (A) and $[(L3Co^{III}\ (^{18}O_2)]^+$ (B), which were generated by addition of 2 equivalents of Et_3N and $H_2{}^{16}O_2$ / $H_2{}^{18}O_2$ (10 equivalents) to **3** in acetonitrile

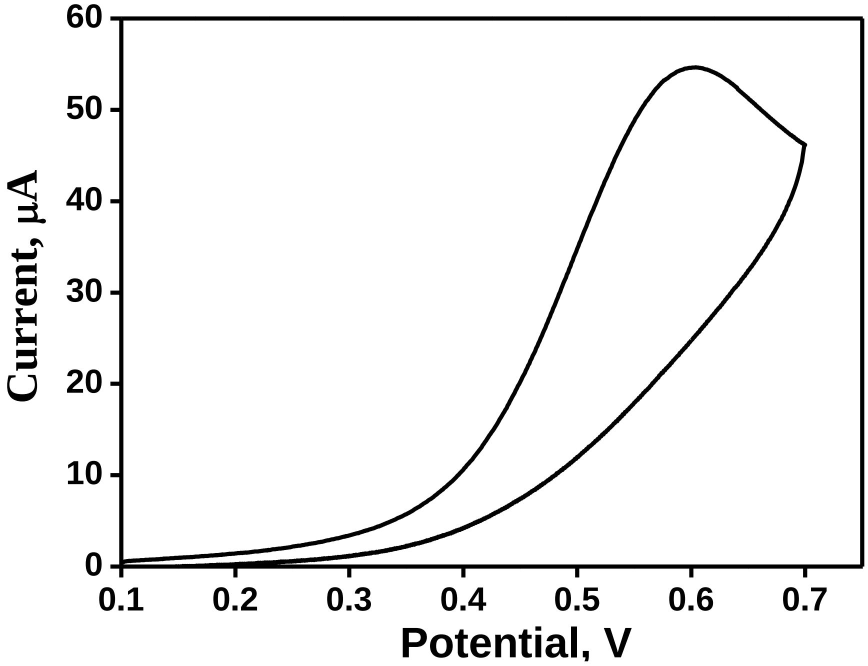

Figure S33. Cyclic Voltammograms of **1** **(**2 ×10^{-3} M) with 2 equivalents of Et_3N and 10 equivalents of H_2O_2 at 25 ºC in acetonitrile. Supporting electrolyte: NBu_4PF_6 (0.2M).

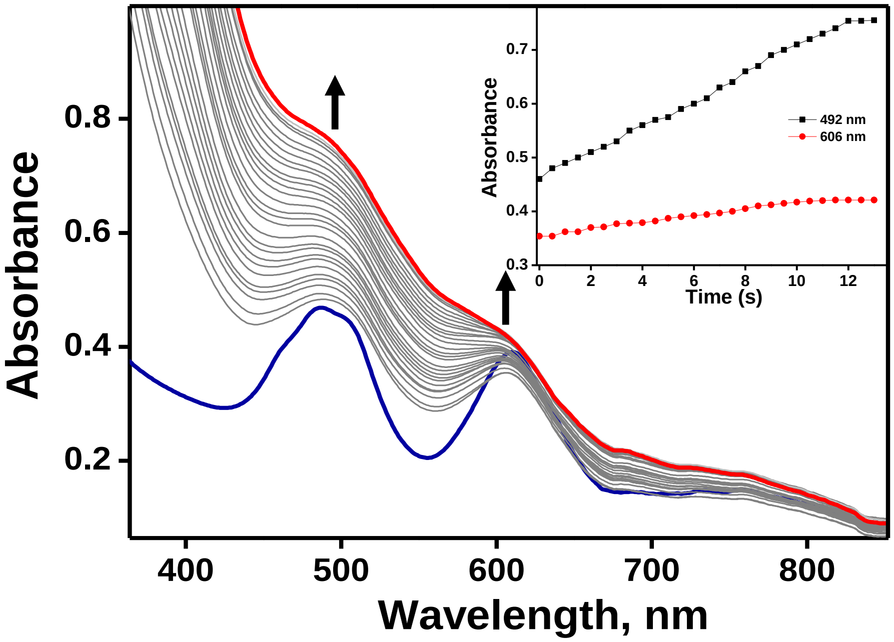

Figure S34. Electronic spectral changes for the reaction of **1** (4 ×10^{-4} M) with 2 equivalents of Et_3N and 30% H_2O_2 (10 equivalents) at -40 °C in acetonitrile solution.

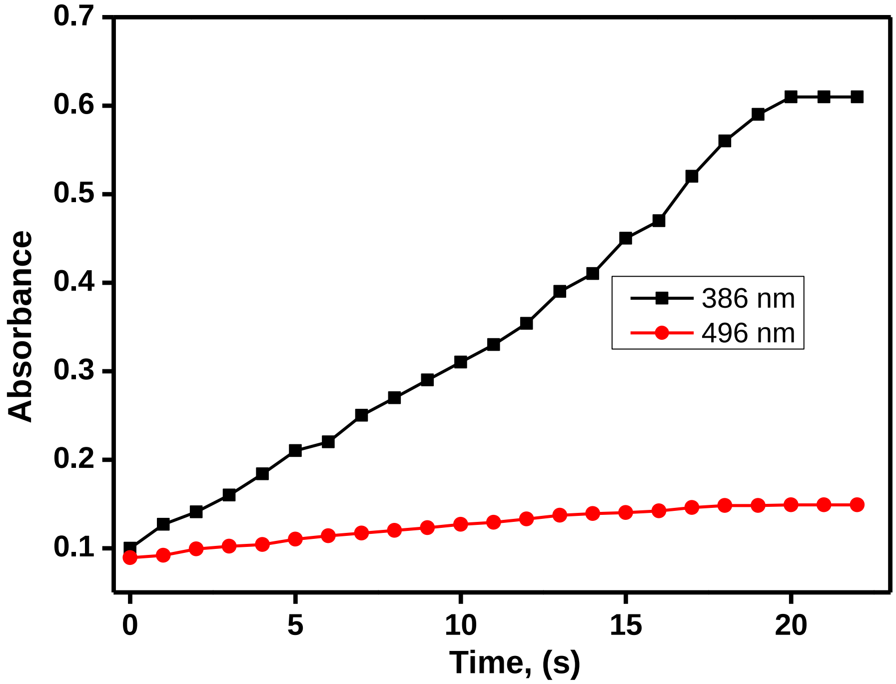

Figure S35. Plot of absorbance vs time for the reaction of **2** with 2 equivalents of Et_3N and 10 equivalents of H_2O_2 (30%)

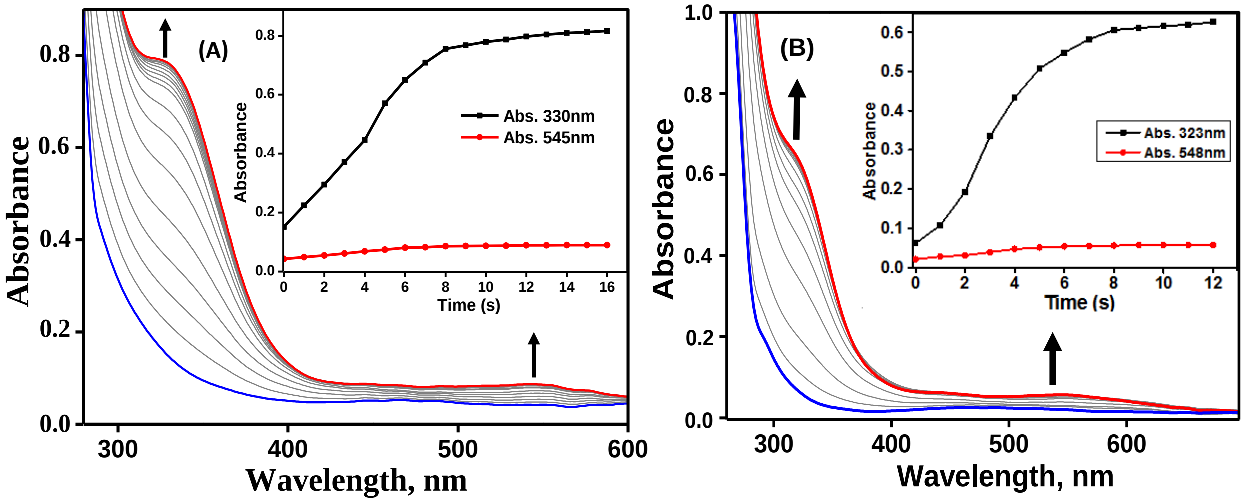

Figure S36. Electronic spectral changes for the reaction of **4** (A)/**5** (B) (4×10^{-4} M) with 2 equivalents of Et_3N and 30% H_2O_2 (10 equivalents) at -40 °C in acetonitrile solution. Insert: plot of absorbance vs time.

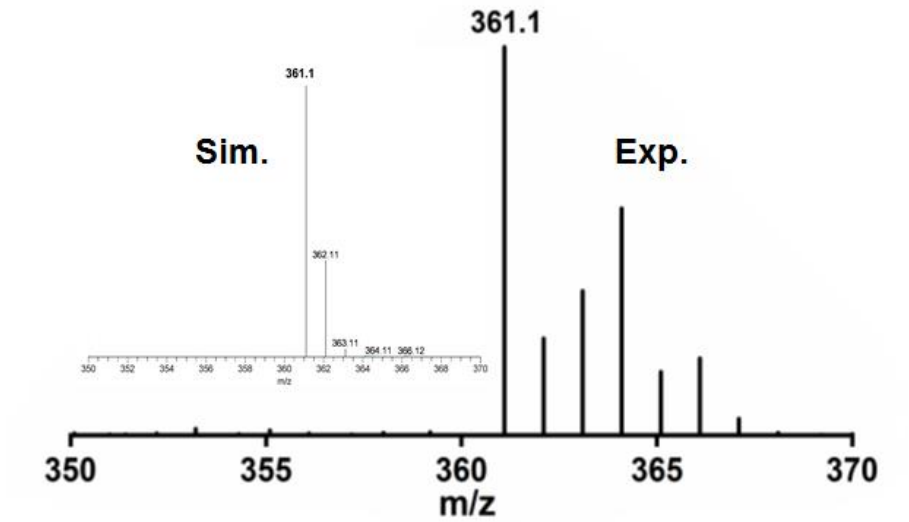

Figure S37. ESI-MS spectra complex **1a** in acetonitrile solution. Insert: calculated *m/z* value: 361.1(**1a**).

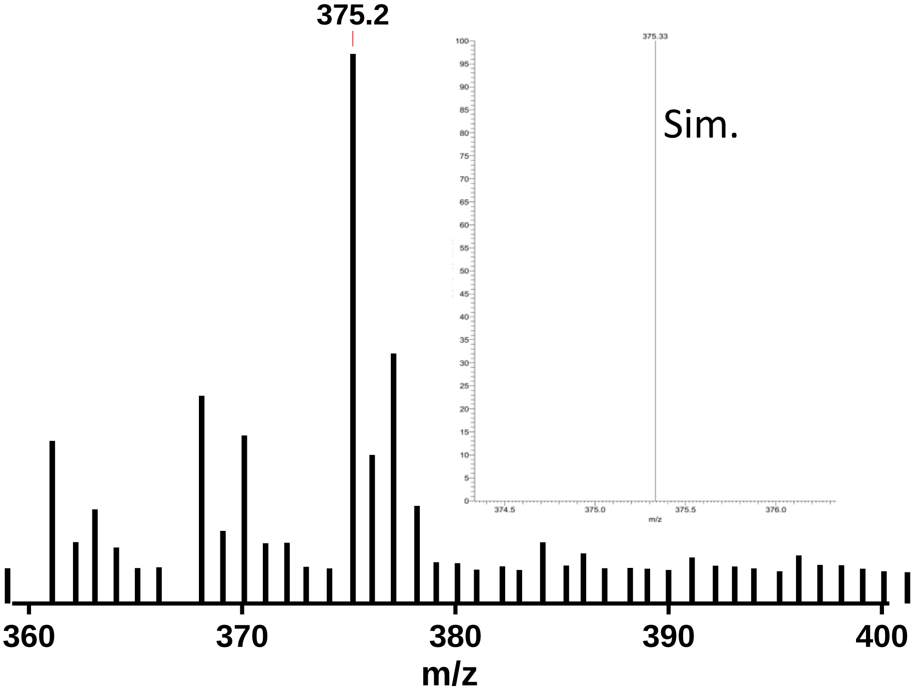

Figure S38. ESI-MS spectra complex **2a** in acetonitrile solution. Insert: calculated *m/z* value: 375.3(**2a**).

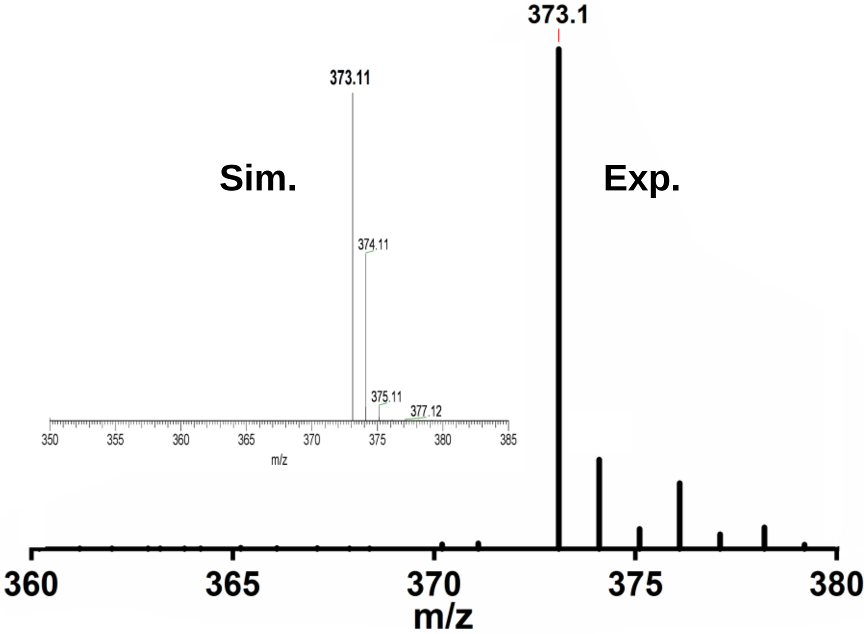

Figure S39. ESI-MS spectra of **4a** and in acetonitrile solution. Insert: Calculated *m/z* value: 373.1(**4a**).

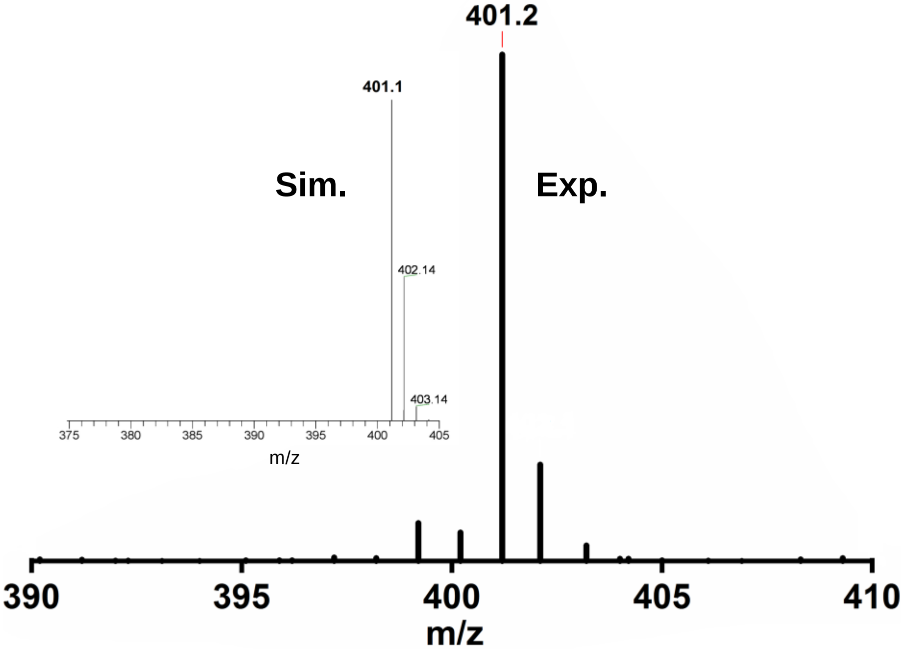

Figure S40. ESI-MS spectra of **5a** in acetonitrile solution. Insert: Calculated *m/z* value: 401.1(**5a**).

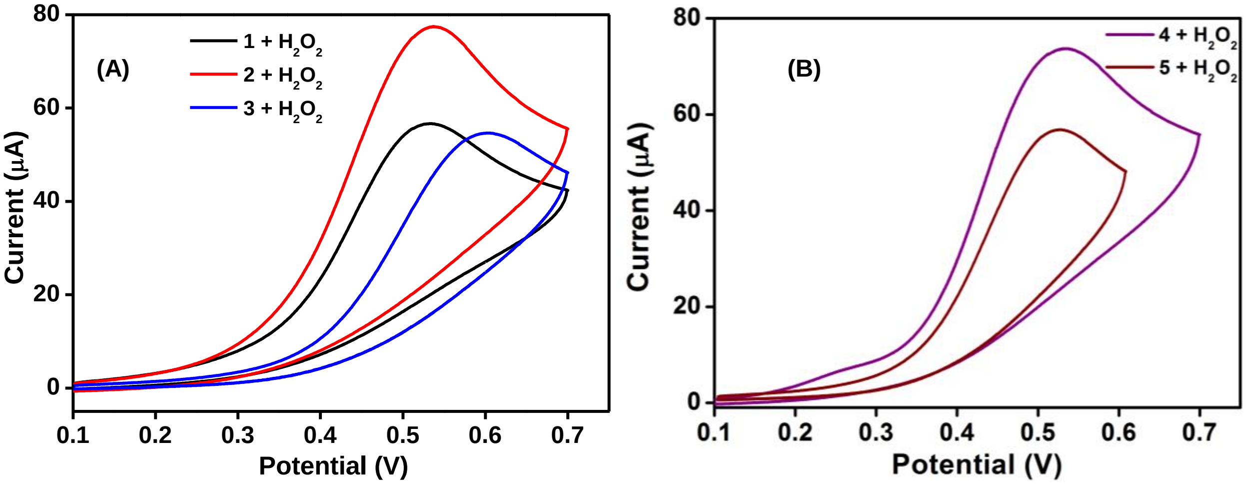

Figure S41. Cyclic voltammograms of **1a - 3a** (A) and **4a - 5a** (B) (2×10^{-3} M) in acetonitrile at 25º C. Supporting electrolyte: NBu_4PF_6 (0.2 M).

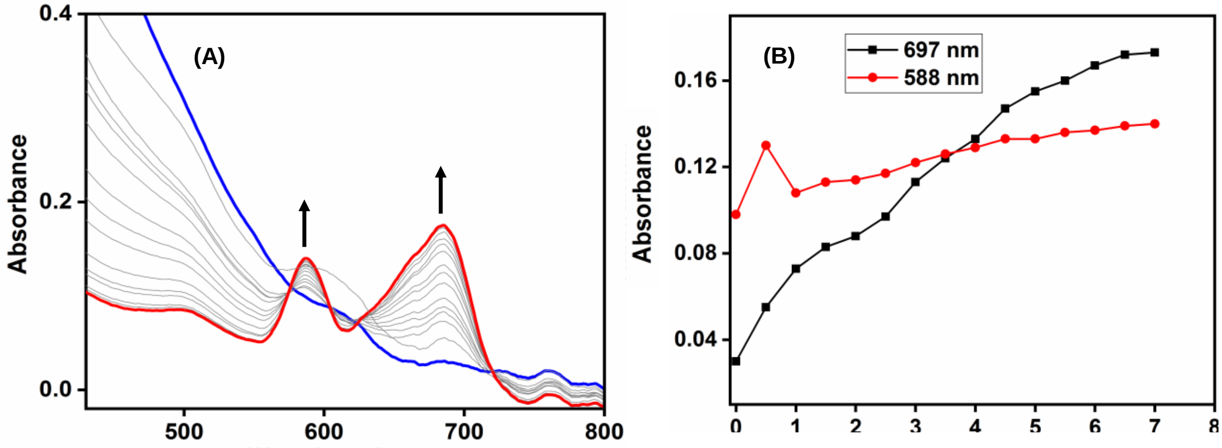

Figure S42. Electronic spectral changes for the reaction of **3a** (4×10^{-4} M) with 3 equivalents of $HClO_4$ at -25 °C in acetonitrile solution (A). plot of absorbance vs. time (B).

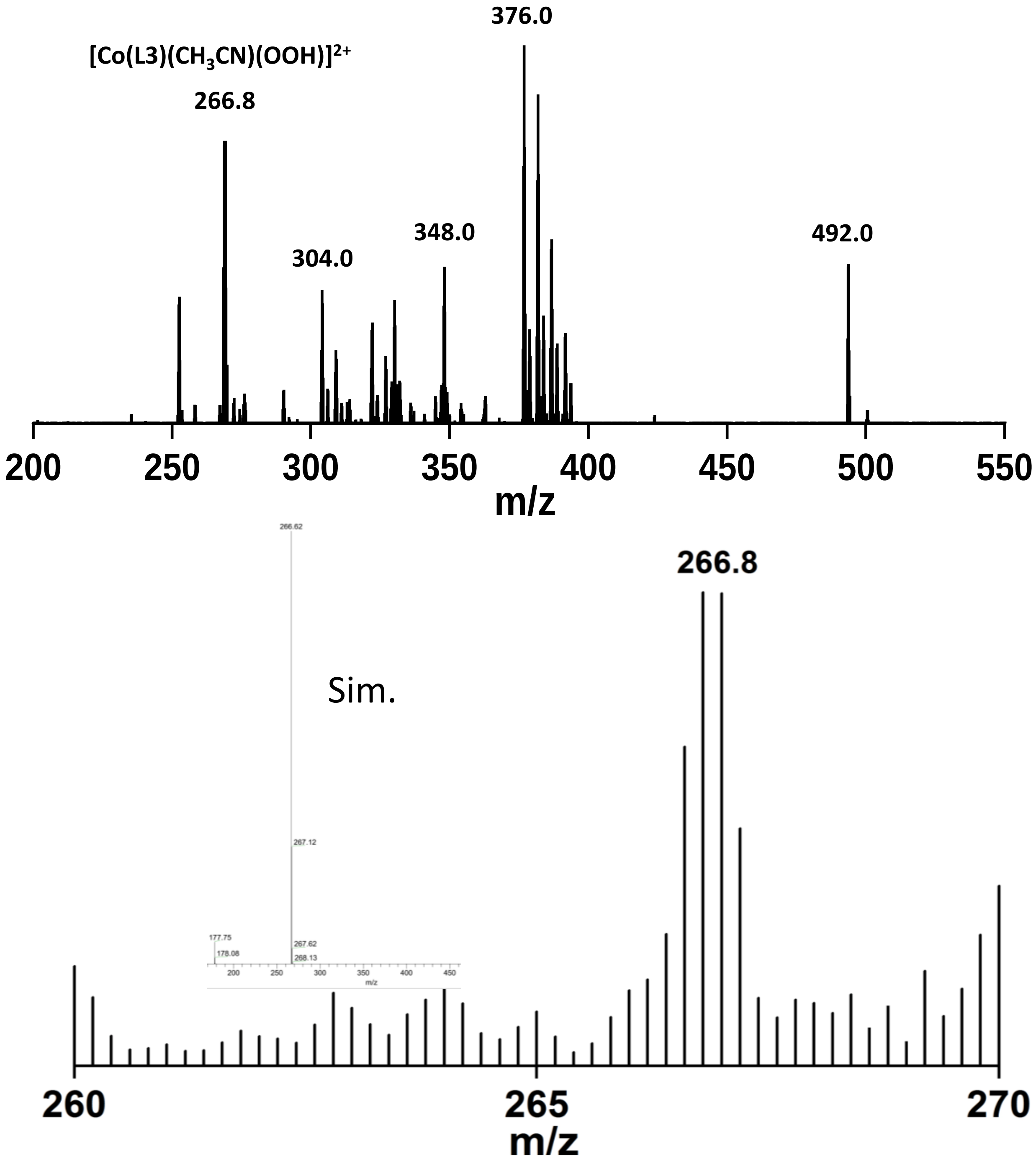

Figure S43. ESI-MS spectra of $[(L3Co^{III})(O_2H)(CH_3CN)]^{2+}$ generated from **3a** with 3 equivalents of $HClO_4$ in acetonitrile. Insert: calculated *m/z* value: 266.62 (**3b**).

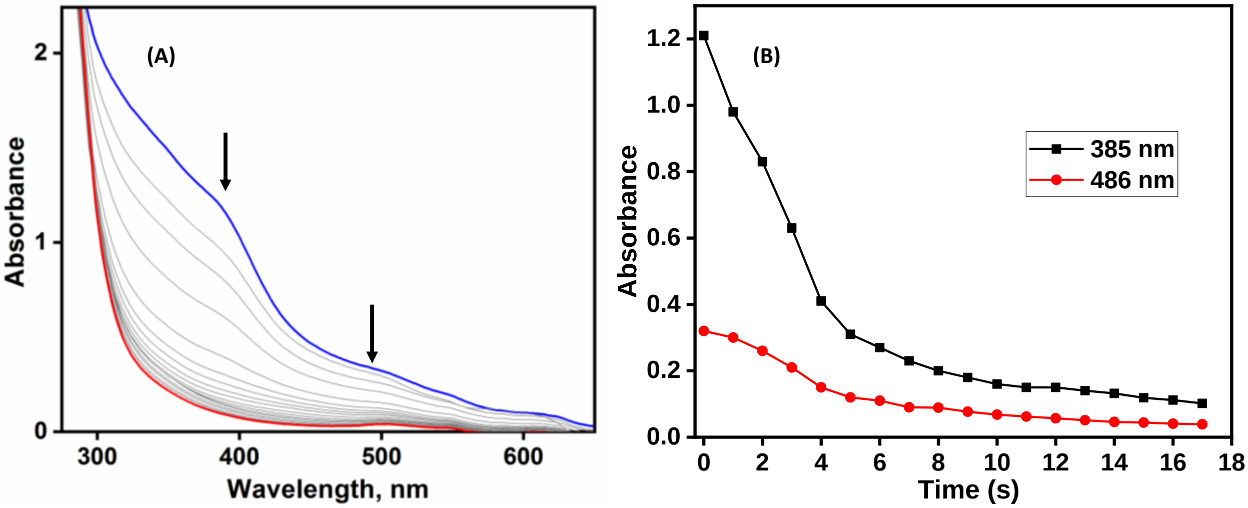

Figure S44. Electronic spectral changes for the reaction of **1a** (4 ×10^{-4} M) with 3 equivalents of $HClO_4$ at -25 °C in acetonitrile solution (A). Plot of absorbance vs. time (B).

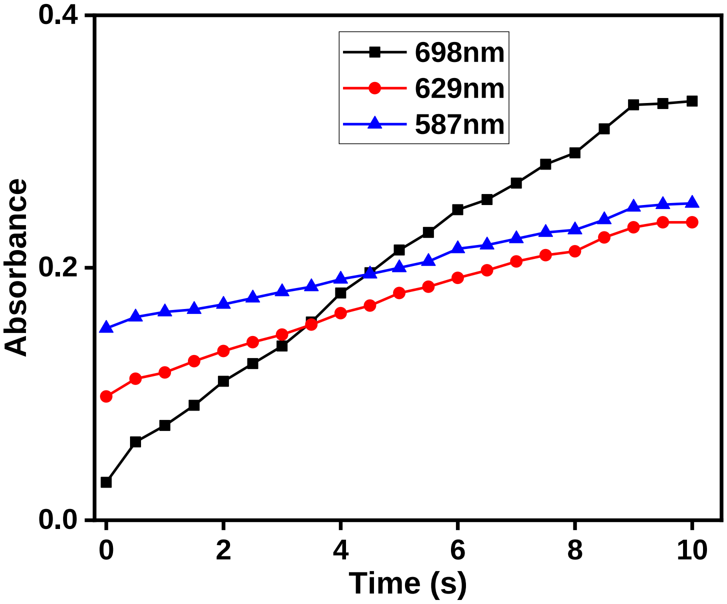

Figure S45. Plot of absorbance at 698, 629, 587 nm vs time for the reaction of **2a** with 3 equivalents of $HClO_4$.

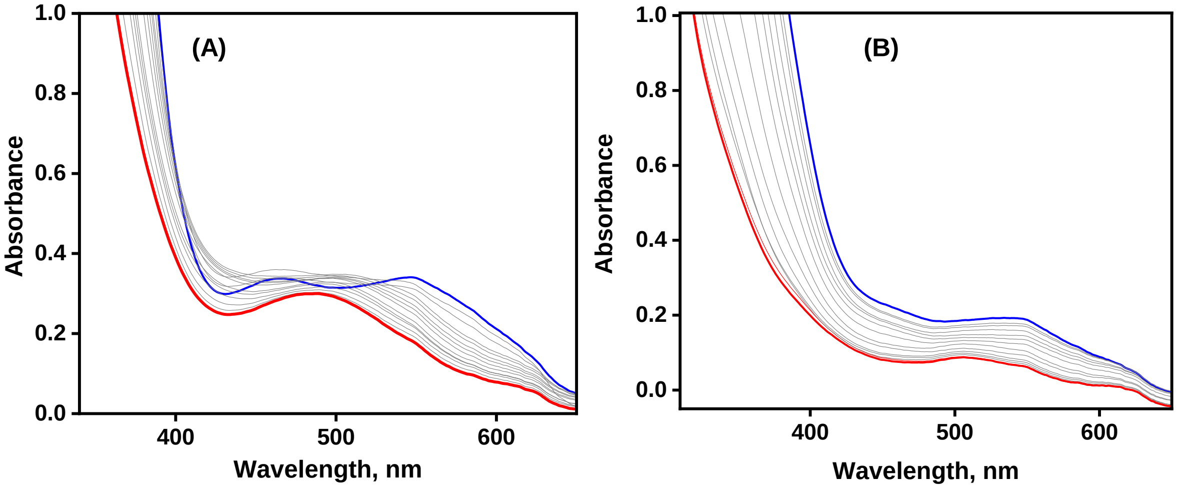

Figure S46. Electronic spectral changes for the reaction of **4a** (A)/**5a** (B) (4 ×10^{-4} M) with 3 equivalents of $HClO_4$ at -25 °C in acetonitrile solution.

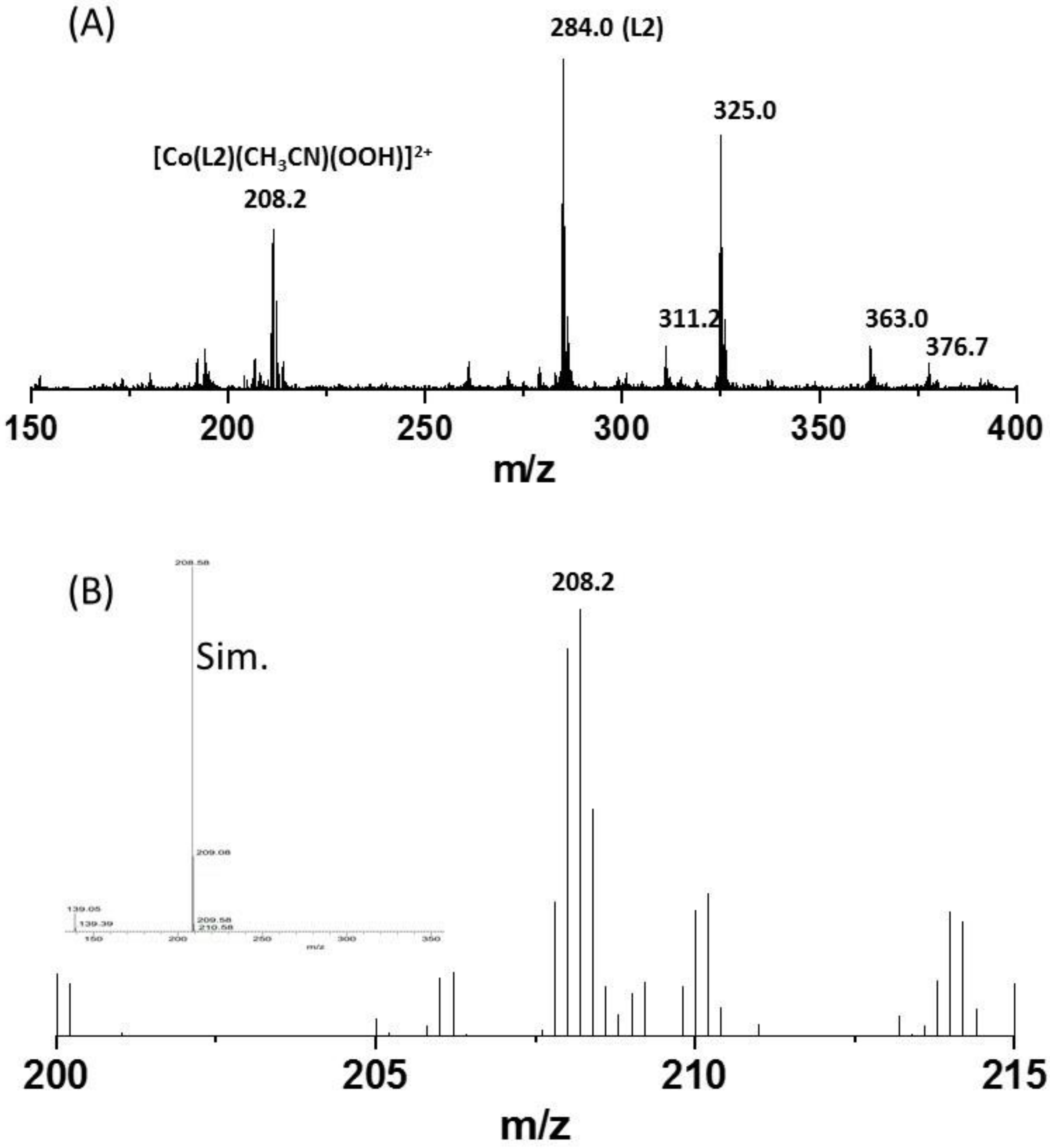

Figure S47. ESI-MS spectra of $[(L2Co^{III})(O_2H)(CH_3CN)]^{2+}$ generated from **2a** with 3 equivalents of $HClO_4$ in acetonitrile. Insert: calculated *m/z* value: 208.58 (**2b**).

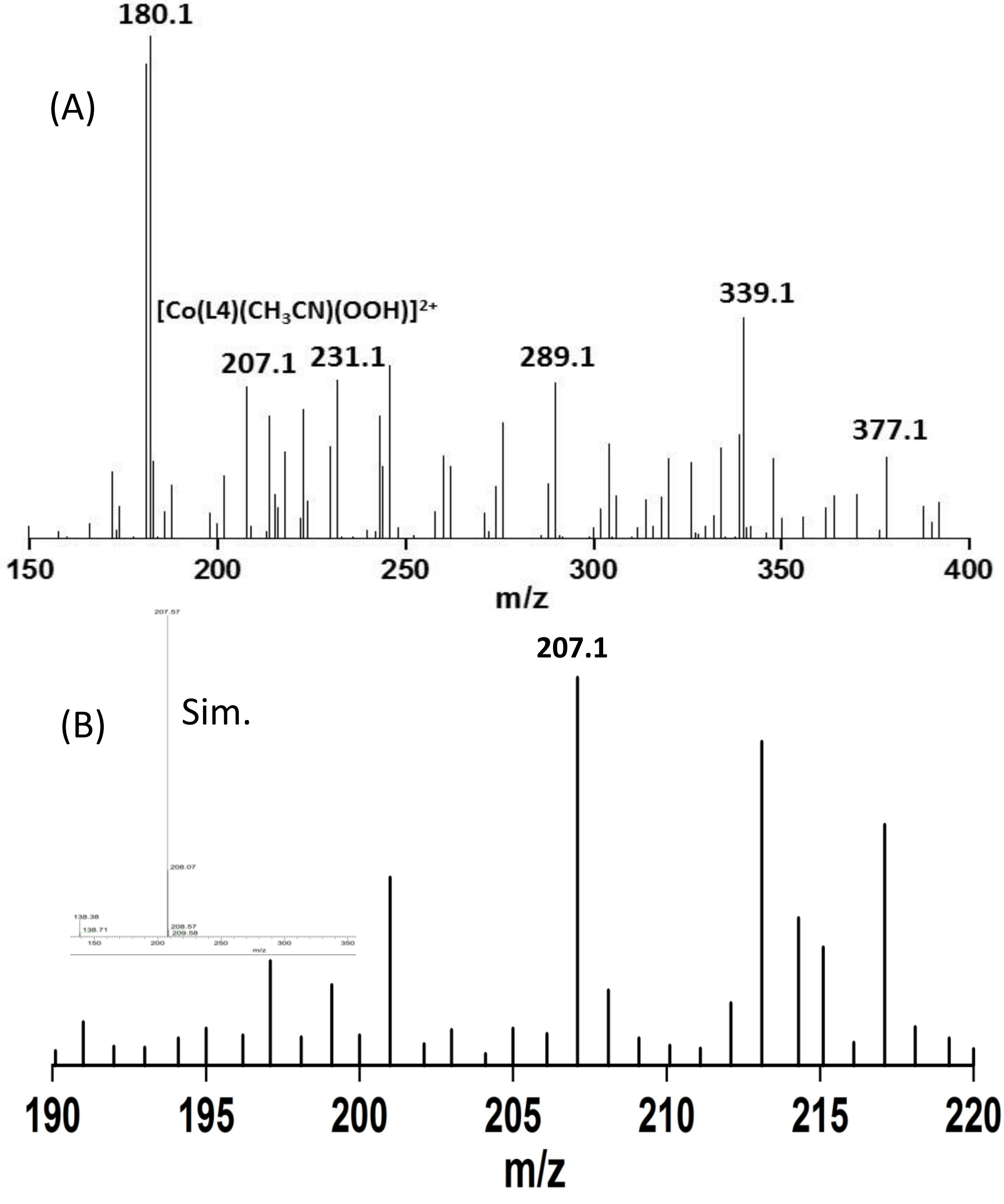

Figure S48. ESI-MS spectra of [(L4Co^{III}) (O$_2$H)(CH$_3$CN)]$^{2+}$ generated from **4a** with 3 equivalents of HClO$_4$ in acetonitrile. Insert: calculated *m/z* value: 207.57 (**4b**).

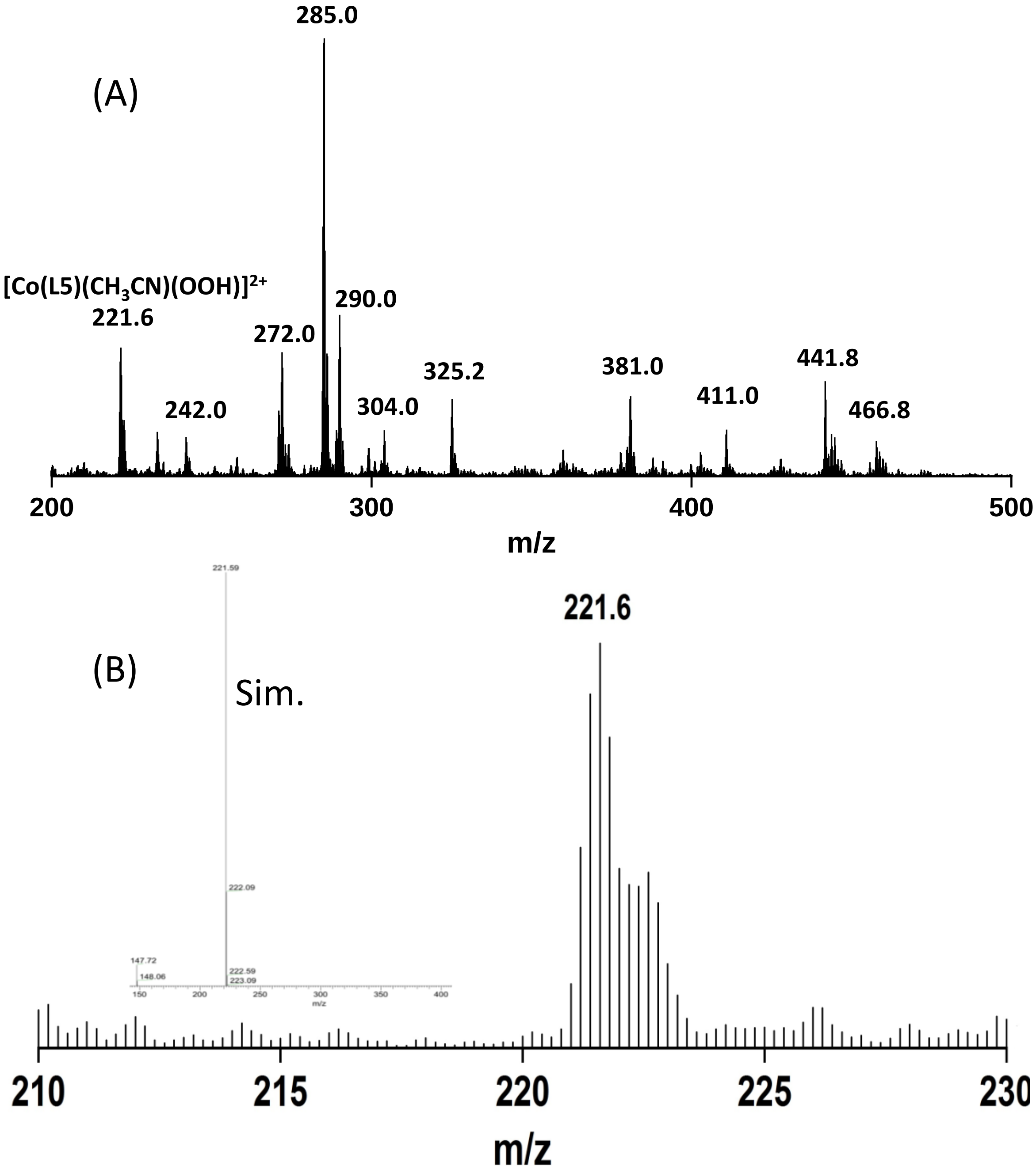

Figure S49. ESI-MS spectra of [(L5Co^{III}) (O$_2$H)(CH$_3$CN)]$^{2+}$ generated from **5a** with 3 equivalents of HClO$_4$ in acetonitrile. Insert: calculated *m/z* value: 221.59 (**5b**).

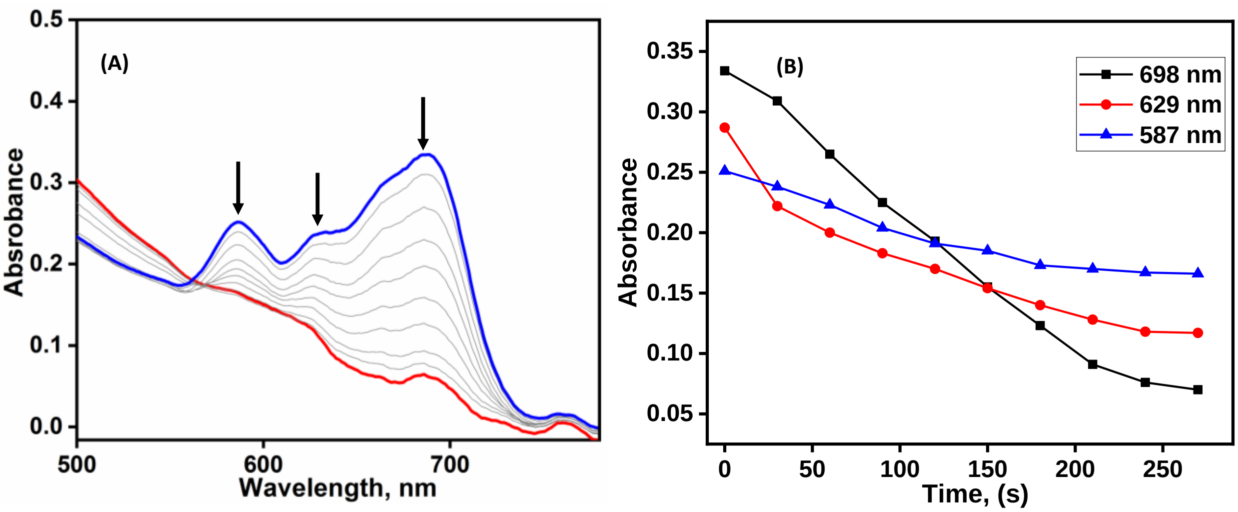

Figure S50. Electronic spectral changes for the reaction of **2b (**4 ×10^{-4} M) with 10 equivalents of benzene at -25 °C in acetonitrile solution (A). Insert: plot of absorbance vs. time (B).

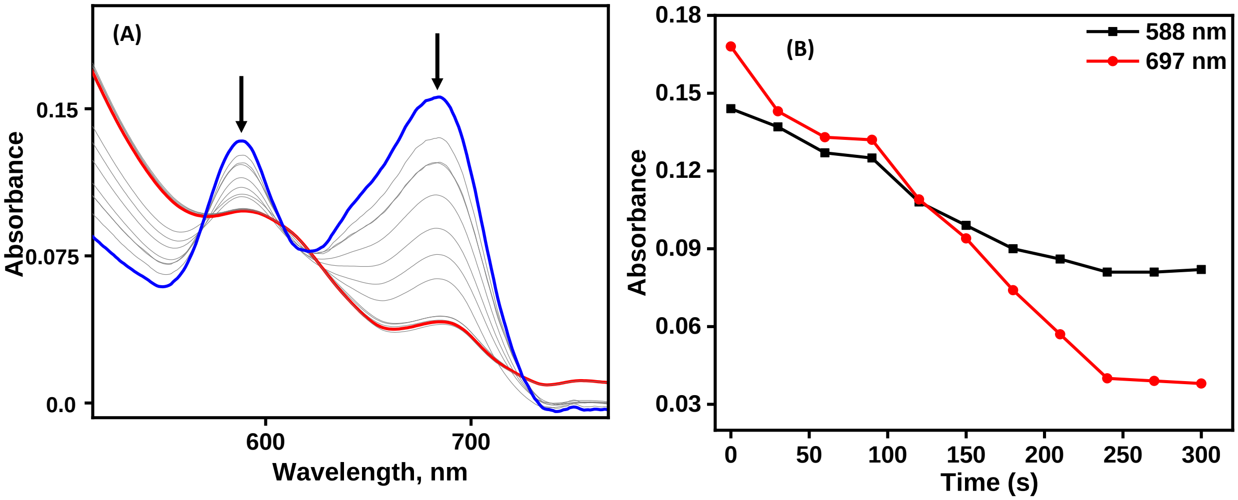

Figure S51. Electronic spectral changes for the reaction of **3b** **(**4 ×10^{-4} M) with 10 equivalents of benzene at -25 °C in acetonitrile solution(A). plot of absorbance vs. time (B).

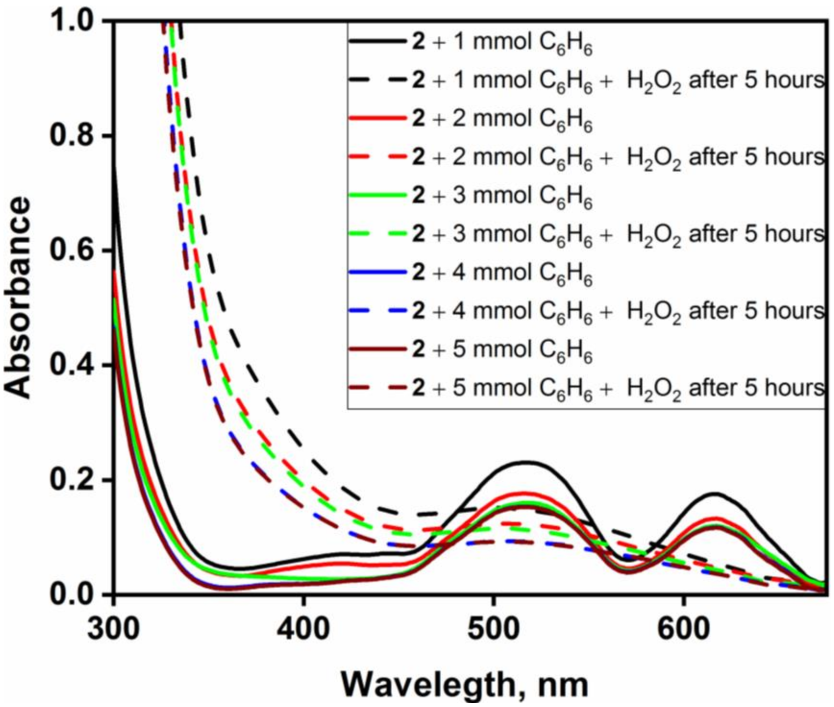

Figure S52. Electronic spectral changes for the reaction of **2** (2.5 μM) with benzene (1 – 5 mmol) and H_2O_2 (25 mmol) at 25 °C in acetonitrile.

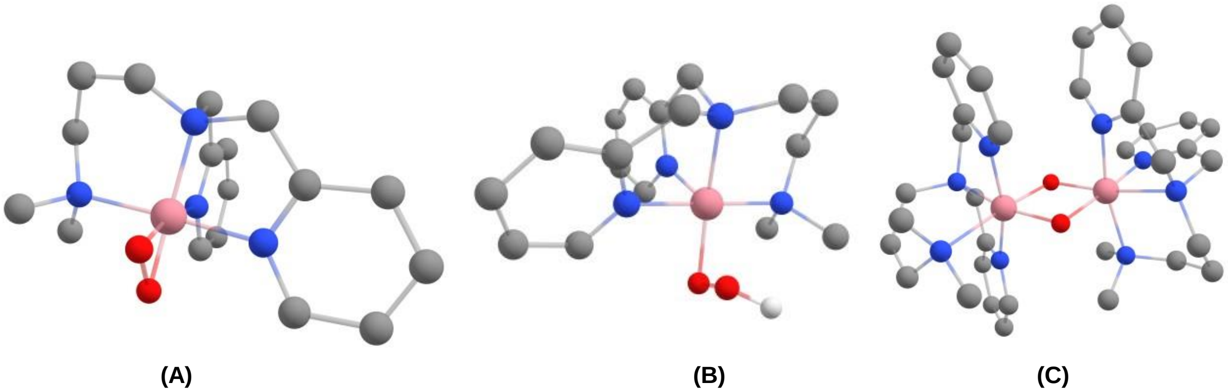

Figure S53. Optimized Structure of $[Co^{III}(L2)(O_2)]^+$ (A), $[Co^{III}(L2)(OOH)]^{2+}$ (B), $[(Co^{III}L2)_2(\mu\text{-}O)_2]^{2+}$ (C) using B3LYP 631-G/ LANL2DZ basis set.

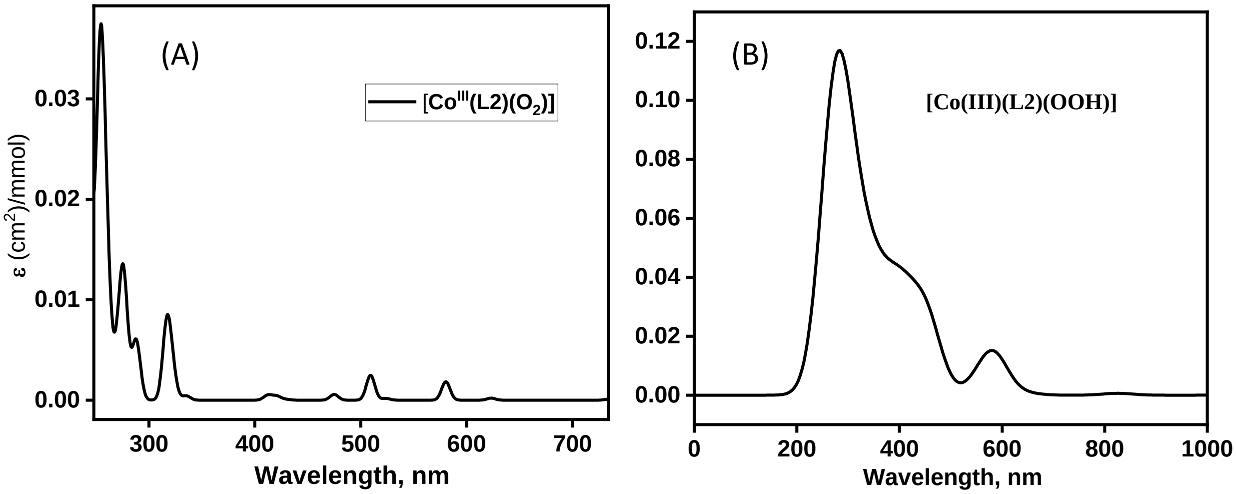

Figure S54. Calculated electronic spectra of [Co^{III}(L2)(O$_2$)]$^{+}$ (A) and [Co^{III}(L2)(OOH)]$^{2+}$ (B) by TDDFT.

Table S1: Selected bond distances^a (Å) and angles (°) of **1** and **1a**

1		**1a**	
Co(1)-N(1)	2.069(5)	Co(2)-N(5)	2.059(4)
Co(1)-N(2)	2.208(4)	Co(2)-N(6)	2.207(4)
Co(1)-N(3)	2.112(4)	Co(2)-N(7)	2.115(4)
Co(1)-N(4)	2.061(5)	Co(2)-N(8)	2.068(5)
Co(1)-Cl(1)	2.2796(14)	Co(2)-Cl(2)	2.2808(13)
N(1)-Co(1)-N(2)	77.50(16)	N(5)-Co(2)-N(6)	78.01(16)
N(1)-Co(1)-N(3)	112.41(19)	N(5)-Co(2)-N(7)	108.2(2)
N(1)-Co(1)-N(4)	110.65(17)	N(5)-Co(2)-N(8)	113.35(17)
N(2)-Co(1)-N(3)	81.50(15)	N(6)-Co(2)-N(7)	81.04(16)
N(4)-Co(1)-N(2)	77.17(17)	N(8)-Co(2)-N(6)	77.32(18)
N(4)-Co(1)-N(3)	125.73(18)	N(8)-Co(2)-N(7)	127.19(17)
N(1)-Co(1)-Cl(1)	102.18(11)	N(5)-Co(2)-Cl(2)	101.59(11)
N(2)-Co(1)-Cl(1)	178.56(11)	N(6)-Co(2)-Cl(2)	179.29(12)
N(3)-Co(1)-Cl(1)	99.91(12)	N(7)-Co(2)-Cl(2)	99.64(11)
N(4)-Co(1)-Cl(1)	101.69(13)	N(8)-Co(2)-Cl(2)	102.35(14)

[a] Standard deviations in parenthesis

Table S2: Selected bond distances[a] (Å) and angles (°) of **2**, **4** and **5.**

	2	**4**	**5**
Co(1)-N(1)	2.043(5)	2.069(3)	2.0823(18)
Co(1)-N(2)	2.254(5)	2.104(3)	2.238(2)
Co(1)-N(3)	2.145(7)	2.143(3)	2.105(2)
Co(1)-N(4)	2.049(5)	2.053(3)	2.099(2)
Co(1)-Cl(1)	2.2814(19)	2.2536(10)	2.2659(7)
N(1)-Co(1)-N(2)	76.7(2)	82.448(11)	82.48(7)
N(1)-Co(1)-N(3)	124.0(2)	156.53(11)	108.45(7)
N(1)-Co(1)-N(4)	117.3(3)	109.22(11)	94.17(7)
N(2)-Co(1)-N(3)	77.7(3)	75.2(11)	75.04(8)
N(2)-Co(1)-N(4)	91.2(3)	126.73(12)	168.93(8)
N(3)-Co(1)-N(4)	112.2(3)	78.82(10)	95.36(8)
N(1)-Co(1)-Cl(1)	97.70(15)	100.36(8)	125.34(5)
N(2)-Co(1)-Cl(1)	167.73(17)	123.46(10)	94.35(5)
N(3)-Co(1)-Cl(1)	97.06(17)	98.36(8)	123.84(6)
N(4)-Co(1)-Cl(1)	101.1(2)	105.77(8)	95.63(6)

[a]Standard deviations in parenthesis

Table S3. Crystal Data and Structure Refinement parameters

	1	**2**	**4**	**5**
Formula	$C_{16}H_{22}Cl_2CoN_4O_4$	$C_{41}H_{44}BClCoN_4$	$C_{17}H_{22}Cl_2CoN_4O_4$	$C_{43}H_{46}BClCoN_4$
Fw	464.20	698.04	476.21	724.03
Cryst system	Monoclinic	Orthorhombic	Monoclinic	Monoclinic
Space group	P21/n	$P2_12_12_1$	P21/c	$P2_1/c$
Temperature	297.06(11)	291.8(5)	295.06(17)	293(2)
a/Å	9.5079(7)	9.8205(9)	12.2832(8)	16.0327(9)
b/Å	32.3832(14)	14.0434(11)	7.3066(5)	10.7162(6)
c/A^0	13.8528(12)	26.706(2)	22.5865(14)	22.6792(12)
$\alpha/^0$	90	90	90	90
$\beta/^0$	110.045(10)	90	95.779(6)	107.025(6)
$\gamma/^0$	90	90	90	90
Volume/$Å^3$	4006.9(6)	3683.1(5)	2016.8(2)	3725.7(4)
Z	8	4	4	4
$\rho_{calc}mg/mm^3$	1.4654	1.1788	1.568	1.291
μ/mm^{-1}	1.150	0.570	1.147	0.569
F(000)	1741.9	1294.4	980.0	1524.0
Reflection collected	11543	8180	7540	13959
Goodness-of-fit on F^2	1.072	1.062	1.049	1.010
R1[a]	0.0760	0.0849	0.0621	0.0736
wR2[b]	0.1697	0.2203	0.1244	0.1096

[a] $R1=\sum\left|\left|F_o\right|-\left|Fc\right|\right|/\sum\left|F_o\right|$, [b] $WR_2=\sum w[(F_o-F_c)^2/\sum w[(F_o^2)^2]^{1/2}$

Table S4. Electronic spectral and redox data for **1 - 5**.

Complex	λ_{max}, nm (ε, M^{-1} cm^{-1})[a]	Redox data[d]				
		Ep_a (V)	Ep_c (V)	ΔE (mV)	$E_{1/2}$ vs. Ag/Ag$^+$	DPV
1	284 (774), 487 (108), 610 (79) 282, 497, 610[b]	0.571	0.426	145	0.498	0.500
2	275 (715), 516 (91), 616 (66) 283, 526, 612[b]	0.586	0.414	172	0.500	0.504
3	274 (694), 472 (70), 597 (64) 284, 479, 605[b]	0.575	0.410	165	0.492	0.508
4	281 (612), 484 (40), 520 (45), 608 (39) 303, 523, 625[b]	0.566	0.374	194	0.496	0.497
5	271 (624), 489 (20) 528 (28), 628 (19) 304, 489, 551, 625[b]	0.563	0.415	148	0.489	0.488

[a]Concentration: 3 × 10^{-3} M in CH_3CN at 25 ºC. [b]solid state Uv-visible spectroscopy. [c]Concentration: complex (4 × 10^{-4} M) in CH_3CN add 2 equi. of Et_3N and 10 equi. 30% H_2O_2 solution at -40˚C. [d]Concentration: 1×10^{-3} M in CH_3CN at 25 ºC. Supporting electrolyte: 0.1 n-$Bu_4NH_4PF_6$; Reference: Ag/Ag$^+$; Working electrode: Glassy carbon; Counter electrode: Pt wire; Scan rate = 100 mV s^{-1}.

Table S5. Optimization of benzene hydroxylation reaction using **3**.

Entry[a]	[H_2O_2] (mmol)	Conversion (%)	Yield (%)	Selectivity (%)
1	5	21	20	95
2	10	23	22	96
3	15	26	24	96
4	20	28	27	96
5	25	30	29	97
6	30	31	29	94
7	35	31	29	94
8	40	32	30	94
9	45	33	30	91
10	50	36	31	86

[a] Reaction condition: benzene (5 mmol), catalyst **3** (5 μmol, 0.1%) and hydrogen peroxide (30%) (5 mmol to 50 mmol) in acetonitrile for 5 hours at 60 °C.

Table S6. Catalytic hydroxylation of benzene using **1 - 5**.

Complex	Temperature (^oC)	Conversion (%)	Selectivity (%)	Yield[a] (%)	TON	TOF (h^{-1})
1	60	20	85	17	172	34
	25	10	90	9	91	18
2	60	20	90	18	183	36
	25	12	92	11	110	22
3	60	21	95	20	200	40
	25	15	94	14	140	28
4	60	15	80	12	122	24
	25	12	83	10	105	23
5	60	16	87	14	137	27
	25	14	86	12	120	22

[a] Reaction condition: benzene (5 mmol), complex (5 μmol, 0.1%) and hydrogen peroxide (30%) (5 mmol) in acetonitrile for 5 hours.

Table S7. Substrate scope for hydroxylation reaction using catalyst **3**.

S. No.	Substrate	Yield (%)	Selectivity (%)		
			P1	P2	P3
1	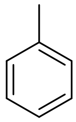	17	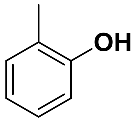 (33%)	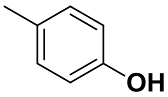 (34%)	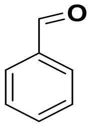 (33%)
2	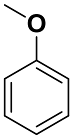	22	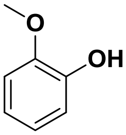 (70%)	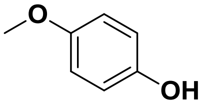 (26%)	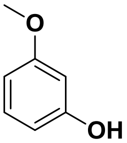 (4%)
3	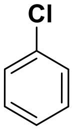	15	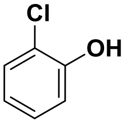 (52%)	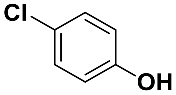 (48%)	-
4	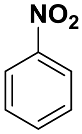	8	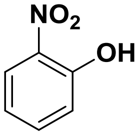 (97%)	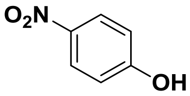 (3%)	-

[a] Reaction condition: Substrate (5 mmol), complex **3** (5 μmol, 0.1%) and hydrogen peroxide (30%) (25 mmol) in acetonitrile for 24 hours at 60 °C.

Table S8. Electronic spectral and redox data for side-on Co(III)-peroxo (**1a – 5a)**[a] and end-on Co(III)-peroxo (**1b - 5b**)[b].

Complex	**λ_{max}, nm (ε, M^{-1} cm^{-1})[a]**	**k_{obs} (× 10^{-2} s^{-1})**	**$t_{1/2}$ (s)**	**E_{pa} (V)**
1a	486 (190),	2.3 ± 0.0003	30	0.532
	605 (88)	0.5 ± 0.0001	138	
1b	501 (125)	-	-	-
2a	386 (1522),	4.6 ± 0.001	15	0.537
	496 (375)	1.5 ± 0.0009	46	
2b	587 (625),	8.7 ± 0.004	8	-
	629 (590),	3.9 ± 0.001	17	
	686 (835)	2.2 ± 0.0003	32	
3a	385 (2280)	1.7 ± 0.0003	40	0.604
	553 (315)			
	576 (275)			
3b	588 (350)	6.9 ± 0.003	10	-
	697 (437)	2.4 ± 0.0029	28	
4a	330(1982),	0.15 ± 0.008	4	0.534
	545(250)	1.2 ± 0.0001	58	
4b	488 (750)	-	-	-
5a	323(900),	0.2 ± 0.015	3	0.531
	548(137)	72 ± 0.00002	96	
5b	506 (217)	-	-	-

[a] Electronic spectral changes for the reaction of complex (**1 - 5**) (4 ×10^{-4} M) with 2 equivalents of Et_3N and 10 equivalents of H_2O_2 at -40°C in acetonitrile solution. [b] Electronic spectral changes for the reaction of side-on Co(III) peroxo complexes (**1a - 5a**) (4 ×10^{-4} M) with 3 equivalents of $HClO_4$ at -25 °C in acetonitrile solution.